

Pan-inhibition of super-enhancer-driven oncogenic transcription by next-generation synthetic ecteinascidins yields potent anti-cancer activity

Received: 25 April 2024

Accepted: 19 December 2024

Published online: 08 January 2025

 Check for updates

Max Cigrang ^{1,2,3,4,10}, Julian Obid ^{1,2,3,4,10}, Maguelone Nogaret ^{1,2,3,4}, Léane Seno^{1,2,3,4}, Tao Ye ^{1,2,3,4}, Guillaume Davidson^{1,2,3,4}, Philippe Catez^{1,2,3,4}, Pietro Berico ^{1,2,3,4,5,6}, Clara Capelli^{1,2,3,4}, Clara Marechal^{1,2,3,4}, Amélie Zachayus^{1,2,3,4}, Clémence Elly^{1,2,3,4}, Marie Jose Guillen Navarro ⁷, Marta Martinez Diez⁷, Gema Santamaria Nunez ⁷, Tsai-Kun Li^{8,9}, Emmanuel Compe ^{1,2,3,4}, Pablo Avilés⁷, Irwin Davidson ^{1,2,3,4}, Jean-Marc Egly^{1,2,3,4,9}, Carmen Cuevas⁷ & Frédéric Coin ^{1,2,3,4} 

The plasticity of cancer cells facilitates their ability to adopt heterogeneous differentiation states, posing a significant challenge to therapeutic interventions. Specific gene expression programs, driven in part by super-enhancers (SEs), underlie cancer cell states. Here we successfully inhibit SE-driven transcription in phenotypically distinct metastatic melanoma cells using next-generation synthetic ecteinascidins. Through functional genomic methodologies, we demonstrate that these compounds inhibit the expression of genes encoding lineage-specific or ubiquitous transcription factors/coactivators by selectively targeting the CpG-rich sequences within their promoters and/or enhancers. This prevents the formation of transcription factor/coactivator condensates necessary for SE-dependent gene expression. Consequently, these compounds exhibit cytotoxic activity across distinct subpopulations of metastatic melanoma cells and inhibit tumor proliferation, including those resistant to current therapies. These findings extend to other cancers, like small cell lung cancer, recently approved for ecteinascidin-based treatment. Overall, our study provides preclinical proof that pan-inhibition of SE-dependent genes with synthetic ecteinascidins is a promising therapeutic approach for tumors with heterogeneous transcriptional landscapes.

In recent years, the concept of ‘transcriptional addiction’ has emerged as a hallmark of cancer cells. Indeed, dysregulated gene expression programs and their associated transcriptional regulatory machinery play crucial roles in sustaining cancer cell phenotypes, thereby rendering them susceptible to transcriptional inhibitors^{1–5}. One of the primary mechanisms contributing to gene expression dysregulation in

cancer cells involves the aberrant acquisition of large clusters of enhancers known as “super-enhancers” (SEs), which drive and maintain the robust expression of oncogenes. SEs are characterized by the aggregated histone modifications H3K27ac and H3K4me1, over longer genomic distances compared to typical enhancers^{6,7}. Moreover, SE-dependent oncogene transcription requires the activity of ubiquitous

A full list of affiliations appears at the end of the paper.  e-mail: fredr@igbmc.fr

transcription factors (e.g., the Cyclin Dependent Kinase 7 (CDK7) of TFIIH) and transcriptional coactivators (e.g., Bromodomain-containing protein 4 (BRD4)), and is maintained by core autoregulatory feedback loops involving master transcription factors and the Mediator complex⁸. Recent evidence has demonstrated that SEs form phase-separated biomolecular condensates, concentrating the transcription apparatus in nuclear puncta to drive the high expression of their regulated oncogenes⁹. Targeting these oncogenic SEs and their spatial organization has emerged as a potential therapeutic strategy¹⁰. Therefore, several compounds aiming to disrupt factors involved in oncogenic SE-driven gene expression, including CDK7 and BRD4 inhibitors, have entered clinical trials^{11,12}. However, they have had limited success due to poor pharmacokinetics and short half-lives^{13–16}.

Cutaneous melanoma is often cited as a prime example of transcriptional addiction due to its frequent dysregulation of specific transcription factors and signaling pathways that drive its aggressive behavior and resistance to treatment^{17–20}. Despite significant advances in developing inhibitors targeting the mutated MAPK signaling pathway (BRAFi and MEKi), along with the introduction of immune checkpoint inhibitors targeting programmed cell death protein 1 (PD-1) and cytotoxic T-lymphocyte-associated antigen 4 (CTLA-4), this cancer remains the most lethal form of skin cancer. Indeed, more than 50% of metastatic melanoma patients either do not initially respond or eventually acquire resistance to these therapies^{21–23}. Melanoma cells evade conventional therapeutic strategies by transitioning between melanocytic/differentiated states, governed by SE-dependent genes essential for cell proliferation, such as the *lineage-specific master transcription factors* *Microphthalmia-associated transcription factor (MITF)* and the *SRY-box transcription factor 10 (SOX10)*, and mesenchymal-like/undifferentiated states, governed by key regulator genes such as the *AXL Receptor Tyrosine Kinase (AXL)* and the *Activator Protein (AP-1)/TEAD* genes implicated in targeted therapy/immunotherapy resistance and invasion^{18,24–30}. This phenotypic adaptation/switch, facilitated by dynamic transcriptional and epigenetic reprogramming mechanisms in response to microenvironmental cues, complicates treatment outcomes^{19,31} and underscores the need for therapeutics that can uniformly target divergent transcription programs governing different tumor cell states³².

Ecteinascidins, a group of natural compounds derived from marine organisms, particularly tunicates, have garnered significant attention due to their anticancer properties³³. Synthetic ecteinascidins refer to compounds that are chemically synthesized to mimic the structure and biological activity of natural ecteinascidins. These synthetic compounds are designed to retain the anticancer properties of natural ecteinascidins while potentially offering advantages such as improved potency, selectivity, and pharmacokinetic properties. A notable member of this class is lurbinectedin, derived from the natural compound trabectedin. Lurbinectedin acts as a DNA binder and transcriptional inhibitor^{34,35}. It is the first molecule approved by the FDA for the treatment of relapsed small-cell lung cancer (SCLC) in the last decade, showcasing the considerable potential of synthetic ecteinascidins as anticancer compounds³⁶.

In this work, in an effort to potentially enhance the benefits of these DNA binders, we develop next-generation synthetic ecteinascidins and test these compounds on melanoma cells due to their well-established transcriptional addiction and propensity for treatment resistance. Our study demonstrates potent anti-proliferative and apoptotic effects of these next-generation DNA binders on differentiated and undifferentiated *BRAF*, *NRAS*, and triple-wild type mutated melanoma cells in various in vitro 2-D and 3-D models and in cell-derived xenograft (CDX) mouse models. We further observe that these compounds potentially inhibit a set of genes encoding ubiquitous transcription factors/coactivators through binding to the CpG islands located in their promoters and/or enhancers. These factors are highly enriched at cell-specific SEs, regulating the expression of cancer-

promoting genes. Consequently, synthetic ecteinascidins disorganize the phase-separated condensates of transcription factors/coactivators, inducing a pan-inactivation of SEs in melanoma cells irrespective of their cell state and driver mutations. This mechanism of action is not observed with BRAFi, MEKi, or DNA-damaging agents such as dacarbazine. Intriguingly, we demonstrate that this uncovered mechanism is also operative in clinically relevant scenarios, such as the treatment of SCLC cells with lurbinectedin, thereby explaining the clinical efficiency of this compound.

Results

Lurbinectedin shows notable efficacy against distinct melanoma cell types

To ascertain the cytotoxic effects of the first-in-class synthetic ecteinascidin lurbinectedin (Fig. 1a) on melanoma cells, we first conducted a dose-response analysis across ten metastatic melanoma cell cultures representing the two primary phenotypes and encompassing the most prevalent driver mutations. We evaluated primary differentiated melanocytic-type cultures derived from patient biopsies, including MM011 (*NRAS*^{Q61K}), MM074 (*BRAF*^{V600E}), MM117 (Triple-wt), alongside commonly used metastatic melanoma cell lines 501mel (*BRAF*^{V600E}), IGR37 (*BRAF*^{V600E}) and SkMel-28 (*BRAF*^{V600E}) (Table 1). These cells demonstrated moderate to high expression levels of the lineage-specific master transcription factors MITF and SOX10, while showing low to undetectable expression levels of the pro-metastatic factors EGFR and AXL^{14,18,37} (Fig. 1b). Additionally, we examined primary undifferentiated metastatic mesenchymal-like melanoma cell cultures derived from patient biopsies, including MM029 (*BRAF*^{V600K}), MM047 (*NRAS*^{Q61R}) and MM099 (*BRAF*^{V600E}), along with the undifferentiated metastatic mesenchymal-like melanoma cell line IGR39 (*BRAF*^{V600E}). These cells exhibited low to undetectable levels of MITF and SOX10, but elevated expression levels of EGFR and/or AXL¹⁴.

We observed varying sensitivities of these metastatic melanoma cells to clinically utilized targeted therapy agents, such as the BRAF inhibitors (BRAFi) vemurafenib and dabrafenib, as well as the MEK inhibitor (MEKi) trametinib (Fig. 1c–e and Table 1). Differentiated *BRAF*^{V600E} melanoma cells were the most responsive to these compounds, whereas undifferentiated cells displayed high resistance. In stark contrast, all melanoma cells showed high sensitivity to lurbinectedin, with IC50 values in the low nanomolar range, from 0.44 to 2.07 nM (Fig. 1f and Table 1). Furthermore, we generated vemurafenib-resistant cells 501mel^{VemUR} and MM074^{VemUR} by exposing initially sensitive cells to increasing drug concentrations in vitro (Fig. 1c and Table 1)¹⁴. These cells acquired a hyperpigmentation phenotype and exhibited cross-resistance to dabrafenib (in the case of MM074^{VemUR}) and trametinib (Fig. 1d, e and Table 1), yet remained highly sensitive to lurbinectedin (Fig. 1f and Table 1).

Collectively, these findings underscore the heightened sensitivity of melanoma cells to lurbinectedin, regardless of cellular phenotypes or driver mutations.

Next-generation ecteinascidins show high cytotoxic effects on melanoma cells

In our pursuit of enhancing the anti-cancer efficacy of synthetic ecteinascidins, we synthesized and assessed next-generation compounds. These molecules, named ecubectedin and PM54, exhibit distinct chemical structures in the non-DNA-binding moieties³⁸. Ecubectedin features a substituted spiro- β -carboline, while PM54 contains a spiro-benzofuropyridine (Fig. 2a, b). Spiro compounds often exhibit enhanced biological activities due to their rigid and three-dimensional structures, which can lead to improved interactions with biological targets. The introduction of a spiro-benzofuropyridine in PM54 is particularly relevant because this moiety was not previously identified in natural ecteinascidins. These unique three-dimensional shapes can contribute to increased selectivity for specific biological

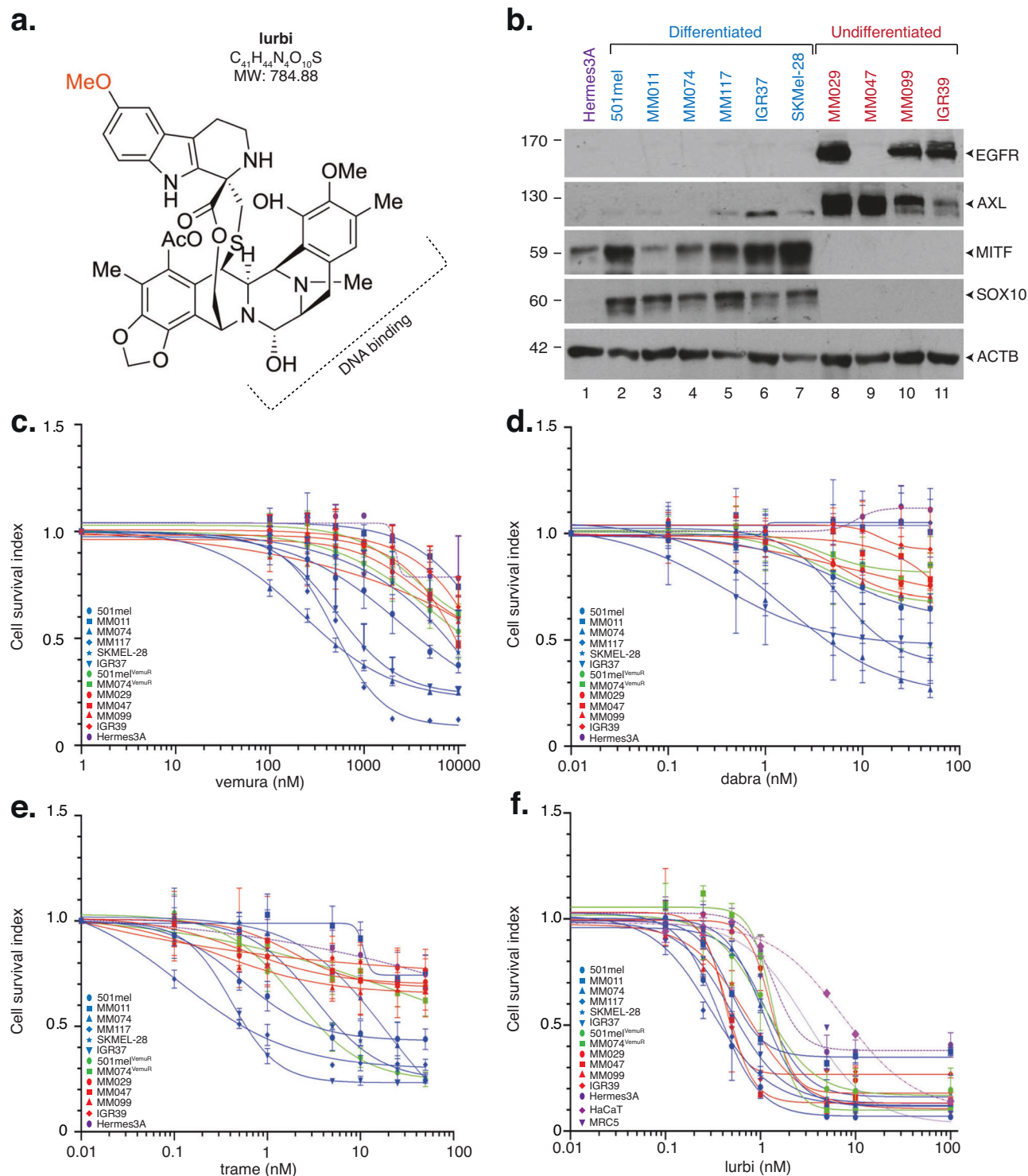


Fig. 1 | Metastatic melanoma cells show high sensitivity to lurbinectedin.

a Chemical structure of lurbinectedin, the first-in-class synthetic ecteinascidin containing tetrahydroisoquinoline subunits. The moiety of the molecule interacting with DNA is indicated. Molecular Weight (MW) is indicated. **b** Protein lysates from either the immortalized Hermes3A melanocytes, differentiated melanoma cells 501mel, MM011, MM074, MM117, IGR37 and SKMel-28 or undifferentiated melanoma cells MM029, MM047, MM099 and IGR39 were immuno-blotted for proteins as indicated. Molecular mass of the proteins is indicated (kDa). Source data are provided as a Source Data file. This experiment was repeated independently three times with similar results. **c–f** Indicated melanoma cells were treated

with increasing concentrations of vemurafenib **c**, dabrafenib **d**, trametinib **e**, or lurbinectedin **f** for 72 h. Mean growth is shown relative to vehicle (DMSO)-treated cells. Error bars indicate mean values \pm Standard Deviation (SD) for three biological replicates. Differentiated (MITF-High, proliferative) melanoma cells are shown in blue, while undifferentiated (MITF-low, invasive) melanoma cells are shown in red. Hyperpigmented melanoma cells with acquired resistance to vemurafenib are shown in green. Immortalized Hermes3A melanocytes, skin keratinocyte HaCaT and embryonic fibroblastic MRC5 cells are shown in violet. Source data are provided as a Source Data file.

Table 1 | Melanoma cell sensitivity against MAPKi and synthetic ecteinascidins

Cells	G	S/T	P	G	vemu	dabra	tram	lurb	ecub	PM54	B-lurb	B-PM54
HaCat	M	WT	Kera	WT	nd	nd	nd	3.2 nM	5.2 nM	10.3 nM	nd	nd
MRC5	M	WT	Fibro	WT	nd	nd	nd	7.5 nM	2.9 nM	12.5 nM	nd	nd
Hermes3A	M	WT	Mel	WT	>10µM	>50 nM	>50 nM	2.7 nM	2.9 nM	4.9 nM	nd	nd
501mel	F	MNS/NS	Diff	BRAF ^{V600E}	2.4µM	>50 nM	3.0 nM	0.4 nM	1.2 nM	1.7 nM	1.4 nM	5.0 nM
MM011	F	LNM/ALM	Diff	NRAS ^{G12R}	>10µM	>50 nM	>50 nM	0.5 nM	1.0 nM	1.4 nM	nd	nd
MM074	F	LNM/SSM	Diff	BRAF ^{V600E}	225 nM	4.7 nM	0.5 nM	1.1 nM	1.1 nM	3.8 nM	nd	nd
MM117	NS	NS/NS	Diff	Triple-WT	490 nM	>50 nM	10.2 nM	0.3 nM	0.7 nM	1.2 nM	nd	nd
SKMEL-28	M	ALN/NS	Diff	BRAF ^{V600E}	>10µM	1.0 nM	5.1 nM	1.2 nM	1.3 nM	1.7 nM	nd	nd
IGR37	M	GLN/NS	Diff	BRAF ^{V600E}	520 nM	25.3 nM	0.5 nM	0.5 nM	1.0 nM	1.5 nM	nd	nd
501mel ^{Vemur}	F	MNS/NS	Pigmented	BRAF ^{V600E}	>10µM	>50 nM	>50 nM	1.1 nM	1.0 nM	2.1 nM	nd	nd
MM074 ^{Vemur}	F	LNM/SSM	Pigmented	BRAF ^{V600E}	>10µM	>50 nM	4.6 nM	1.3 nM	1.6 nM	3.1 nM	nd	nd
MM029	F	LNM/SSM	Undiff	BRAF ^{V600K}	>10µM	>50 nM	>50 nM	1.3 nM	1.4 nM	4.7 nM	1.4 nM	6.0 nM
MM047	M	NS/NS	Undiff	NRAS ^{G12R}	>10µM	>50 nM	>50 nM	0.4 nM	0.9 nM	1.4 nM	nd	nd
MM099	M	LT/NS	Undiff	BRAF ^{V600E}	>10µM	>50 nM	>50 nM	0.7 nM	1.4 nM	1.8 nM	nd	nd
IGR39	M	LT/SSM	Undiff	BRAF ^{V600E}	>10µM	>50 nM	>50 nM	0.4 nM	0.8 nM	0.8 nM	nd	nd
MM074+ INFY	F	LNM/SSM	Pseudo-Inter	BRAF ^{V600E}	8µM	ns	ns	0.9 nM	1.0 nM	1.0 nM	nd	nd

IC50 of vemurafenib (vemu), dabrafenib (dabra), trametinib (tram), lurbicetinid (lurb), ecubectedin (ecub) and PM54 against various melanoma cells. The gender (G) of the patient, site and tumor type (S/T), phenotype (P) and genotype (G) of these cells are indicated. Hermes3A are transformed melanocytes. WT= Wild-type; NS= Not Specified, MNS= Metastatic, Not Specified. LNM= Lymph Node Metastasis, SSM= Superficial Spreading Melanoma, ALN= Axillary Lymph Node, LT= Left Thigh, GLN= Groin Lymph Node, nd= Not Determined. IC50 of Bio-lurb (B-lurb) and Bio-PM54 (B-PM54) are also indicated.

targets, reducing off-target effects and warranting further investigation. We observed that all melanoma cells displayed high sensitivity to these next-generation synthetic ecteinascidins, with IC50 values in the low nanomolar range, spanning from 0.7 to 5 nM (Fig. 2c, d and Table 1). Notably, the non-cancerous Hermes3A immortalized melanocytes, the skin keratinocyte HaCaT cells, and the embryonic fibroblastic MRC5 cells were consistently 3- to 7-times less sensitive to synthetic ecteinascidins compared to melanoma cells.

These findings demonstrate that the next-generation synthetic ecteinascidins exhibit high cytotoxic effects on a range of melanoma cells containing distinct driver mutations and cellular phenotypes.

Synthetic ecteinascidins induce melanoma cell apoptotic death

We next compared the efficacy of synthetic ecteinascidins on cell proliferation and survival. Clonogenic assays demonstrated a significant impact of these molecules on all tested metastatic melanoma cell cultures or cell lines (Fig. 3a), accompanied by a significant inhibition of melanoma cell proliferation (Fig. 3b). Concurrently, there was a notable blockade of cell cycle progression in the G2/M phase (Fig. 3c) and induction of apoptosis (Fig. 3d). The compounds also significantly inhibited the invasion capacities of undifferentiated metastatic melanoma cell cultures (Fig. 3e). Lurbicetinid is known to trigger a DNA damage response characterized by the activation of γH2AX due to drug-induced DNA breaks³⁴. Using immunofluorescence, we observed γH2AX accumulation in differentiated 501mel or undifferentiated MM029 cells upon treatment with the three synthetic ecteinascidins (Supplementary Fig. 1a–d), which was confirmed by immunoblotting (Supplementary Fig. 1e). In parallel, phosphorylation of the protein kinase ataxia telangiectasia mutated (ATM), the master damage response protein, was observed in these cells (Supplementary Fig. 1e). Of note, MAPKi did not induce activation of γH2AX in sensitive 501mel cells.

We further employed 3-D melanosphere culture assays to assess the response of melanospheres derived from the melanocytic-like MM074 cells to BRAFi and MEKi. In sharp contrast to the response observed in 2-D cultures, BRAFi and MEKi failed to reduce cell viability in the 3-D cultures, even at doses equivalent to 5x of the IC50 concentrations determined in 2-D (Supplementary Fig. 2a). Conversely, synthetic ecteinascidins demonstrated significant cytotoxic effects on MM074 melanospheres (Supplementary Fig. 2b), inducing apoptosis at nanomolar concentrations (Supplementary Fig. 2c). These findings elucidate the pro-apoptotic impacts of synthetic ecteinascidins on both differentiated and undifferentiated melanoma cells cultured in 2- or 3-D settings.

Synthetic ecteinascidins exhibit robust anti-tumor activities

The above data prompted us to examine the impact of synthetic ecteinascidins on melanoma cell-derived xenograft (CDX) mouse models. We first monitored the tumor volumes following intravenous (IV) administration of synthetic ecteinascidins once per week for three consecutive weeks at a concentration of 1.2 mg/kg. Treatments commenced (d.0) when the tumors reached 150 mm³ in athymic nude female mice aged 4 to 6 weeks (*n*=10/group) and finished fourteen days later (d.14). We tested CDXs obtained from two highly proliferative melanoma cell lines widely used for drug screening (LOX-IMVI^{BRAF-V600E} and WM-266-4^{BRAF-V600D})³⁹. For both CDXs, we observed significant tumor growth regression upon treatment with synthetic ecteinascidins, starting d.5 (Fig. 4a, b). The tumor growth delay was persistent even after d.14 when treatment was withdrawn, and lasted until d.25, emphasizing a period of latency of 10 days following the end of the treatment. Simultaneously, a marked augmentation in overall survival was observed, predominantly evident during the latency phase (Fig. 4c, d).

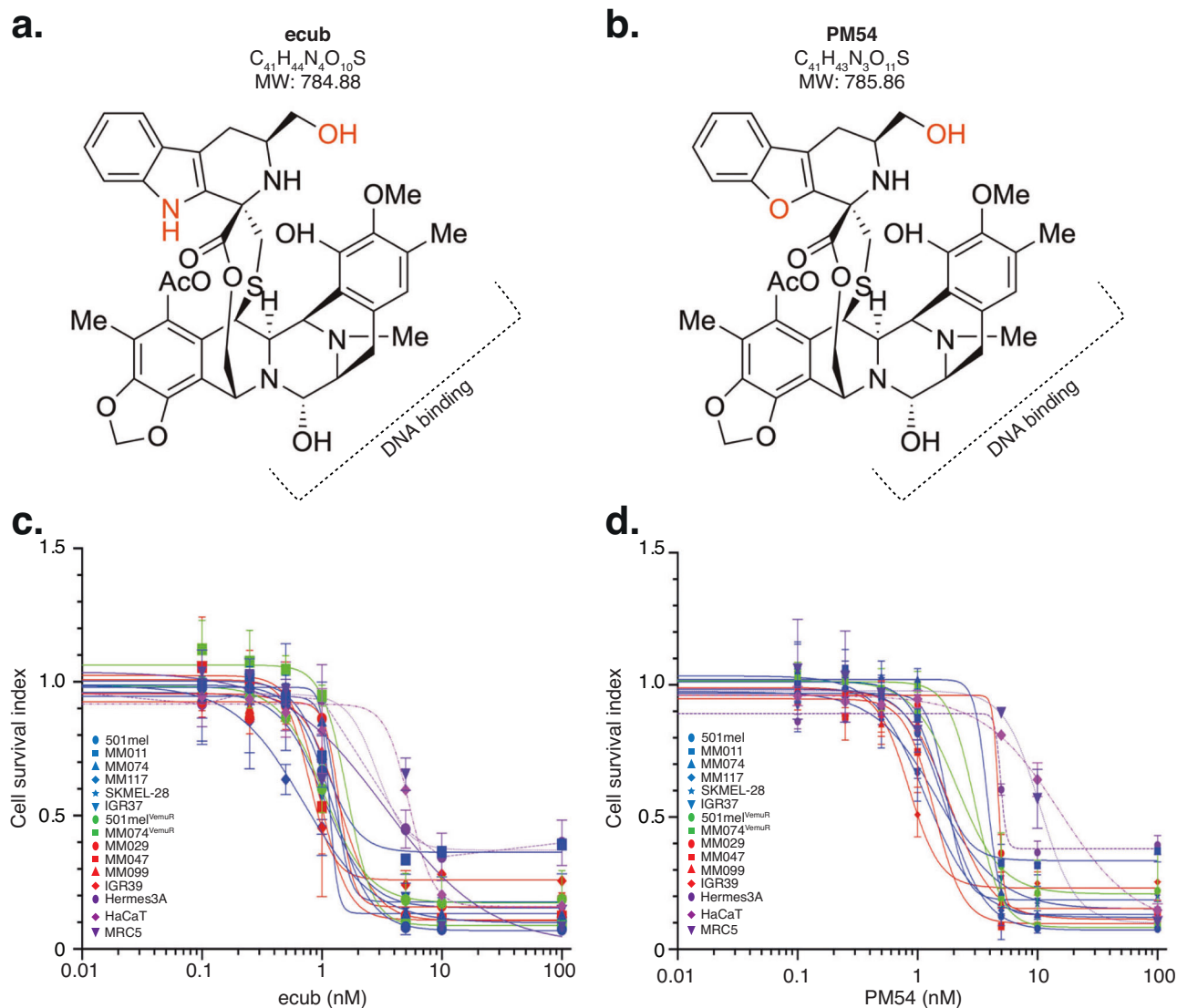


Fig. 2 | Metastatic melanoma cells show high sensitivity to next-generation synthetic ecteinascidins. **a, b** Chemical structure of ecubectedin **a** and PM54 **b**, two next-generation synthetic ecteinascidins analogs of lurbinectedin. The modifications are highlighted in red. The moiety of the molecule interacting with DNA is indicated. Molecular Weight (MW) is indicated. **c, d** Indicated melanoma cells were treated with increasing concentrations of ecubectedin **c** or PM54 **d**, for 72 h. Mean growth is shown relative to vehicle (DMSO)-treated cells. Error bars

indicate mean values \pm Standard Deviation (SD) for three biological triplicates. Differentiated (MITF-High, proliferative) melanoma cells are shown in blue, while undifferentiated (MITF-low, invasive) melanoma cells are shown in red. Hyperpigmented melanoma cells with acquired resistance to vemurafenib are shown in green. Immortalized Hermes3A melanocytes, skin keratinocyte HaCaT and embryonic fibroblastic MRC5 cells are shown in violet. Source data are provided as a Source Data file.

We next analyzed the effect of the drugs on MAPKi-resistant cells using the 501mel and 501mel^{Vemur} cells. Once the tumors reached a size of 150 mm³ in female NSG mice, a single IV dose of either ecubectedin or PM54 at a concentration of 1.2 mg/kg was administered to the animals ($n = 8$ /group). Twenty-four hours after this single IV dose, we assessed the mitotic or apoptotic indexes on tumor sections using immunostaining of phospho-histone H3 (pHH3) or caspase-3 cleavage, respectively⁴⁰. We observed a significantly decreased mitotic index and increased apoptosis upon treatment with synthetic ecteinascidins, for CDXs derived from both 501mel and 501mel^{Vemur} (Supplementary Fig. 3a–d). Consequently, we observed that treatments with synthetic ecteinascidins significantly impacted the tumor growth of CDXs derived from 501mel and 501mel^{Vemur} melanoma cells (Figs. 4e and 2f) and increased the overall survival of the mice (Fig. 4g, h). Altogether, these studies suggest that synthetic ecteinascidins are highly active at inhibiting the growth and inducing apoptosis in melanoma tumors in vivo, even in those presenting resistance to clinically relevant treatments.

Synthetic ecteinascidins affect the expression of cancer-promoting genes

Given the proposed impact of lurbinectedin on transcription³⁵, we conducted gene expression profiling (RNA-Seq) in 2-D cultures of differentiated and undifferentiated melanoma cells. Following the treatment with synthetic ecteinascidins, major transcriptional effects were observed, with a large number of genes being downregulated for both cell types, and a lesser number of genes being upregulated (Supplementary Fig. 4a–c and Supplementary Data 1). However, significant differences in the types of genes being affected in either differentiated or undifferentiated cells were observed. Among the downregulated genes, we noted the presence of several cancer-promoting genes such as *MITF*, *Paired Box 3 (PAX3)* or *SOX10* specifically in differentiated melanoma cells or *AXL*, *Epidermal Growth Factor Receptor (EGFR)*, *SRY-Box Transcription Factor 9 (SOX9)*, *FOS Like 2 (FOSL2)* and *TEAD4* specifically in undifferentiated cells. These data were confirmed in 2-D models by RT-qPCR and/or immunoblotting (Supplementary

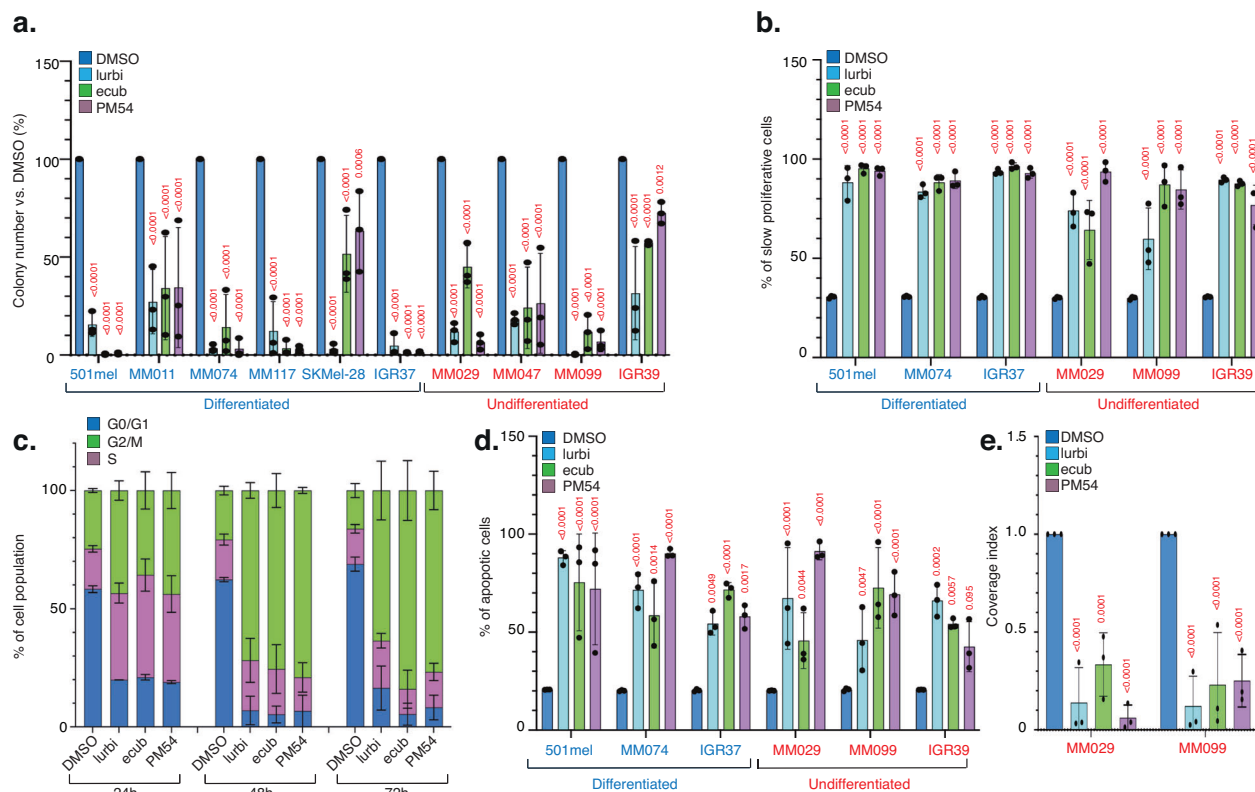


Fig. 3 | Synthetic ecteinascidins induce cell cycle arrest and apoptosis.

a Metastatic melanoma cells were treated with either vehicle (DMSO), lurbinectedin, ecubectedin or PM54 (1xIC50 concentration, 48 h) and allowed to grow for additional 10 days in the absence of drugs. Results are shown as the mean colony numbers \pm SD for three biological triplicates. Ordinary one-way ANOVA using Dunnett's multiple comparisons test was used to determine the p -values (vs. DMSO). Source data are provided as a Source Data file. **b** Metastatic melanoma cells were incubated with CellTrace and subsequently treated with either vehicle (DMSO), lurbinectedin, ecubectedin or PM54 (1xIC50 concentration, 72 h). Quantifications of populations with high CellTrace signal in DMSO or drug-treated cells are shown as mean values \pm SD for three biological triplicates. Proliferative cells show low CellTrace signal while non proliferative cells show high CellTrace signal. Ordinary one-way ANOVA using Dunnett's multiple comparisons test was used to determine the p -values (vs. DMSO). Source data are provided as a Source Data file. **c** 501mel cells were treated with either vehicle (DMSO), lurbinectedin, ecubectedin

or PM54 (1xIC50 concentration, 72 h). Cell cycle was studied by propidium iodide staining and flow cytometry, and results are shown as mean values \pm SD for three biological triplicates. Source data are provided as a Source Data file. **d** Metastatic melanoma cells were treated with either vehicle (DMSO), lurbinectedin, ecubectedin or PM54 (1xIC50 concentration, 72 h). Apoptosis was studied by flow cytometry using annexin V-APC staining. Results are shown as mean values \pm SD for three biological triplicates. Ordinary one-way ANOVA using Dunnett's multiple comparisons test was used to determine the p -values (vs. DMSO). Source data are provided as a Source Data file. **e** MM029 and MM099 metastatic melanoma cells were treated with either vehicle (DMSO), lurbinectedin, ecubectedin or PM54 (1xIC50 concentration, 48 h). Invasion was determined using Boyden chamber assays. Results are shown as mean values of coverage index \pm SD for three biological triplicates. Ordinary one-way ANOVA using Dunnett's multiple comparisons test was used to determine the p -values (vs. DMSO). Source data are provided as a Source Data file.

Fig. 5a–d) and in 3-D models by RT-qPCR (Supplementary Fig. 5e,f). Collectively, our findings underscore the significant and partially cell-type-specific inhibition of expression of cancer-promoting genes in metastatic melanoma cells upon treatment with synthetic ecteinascidins.

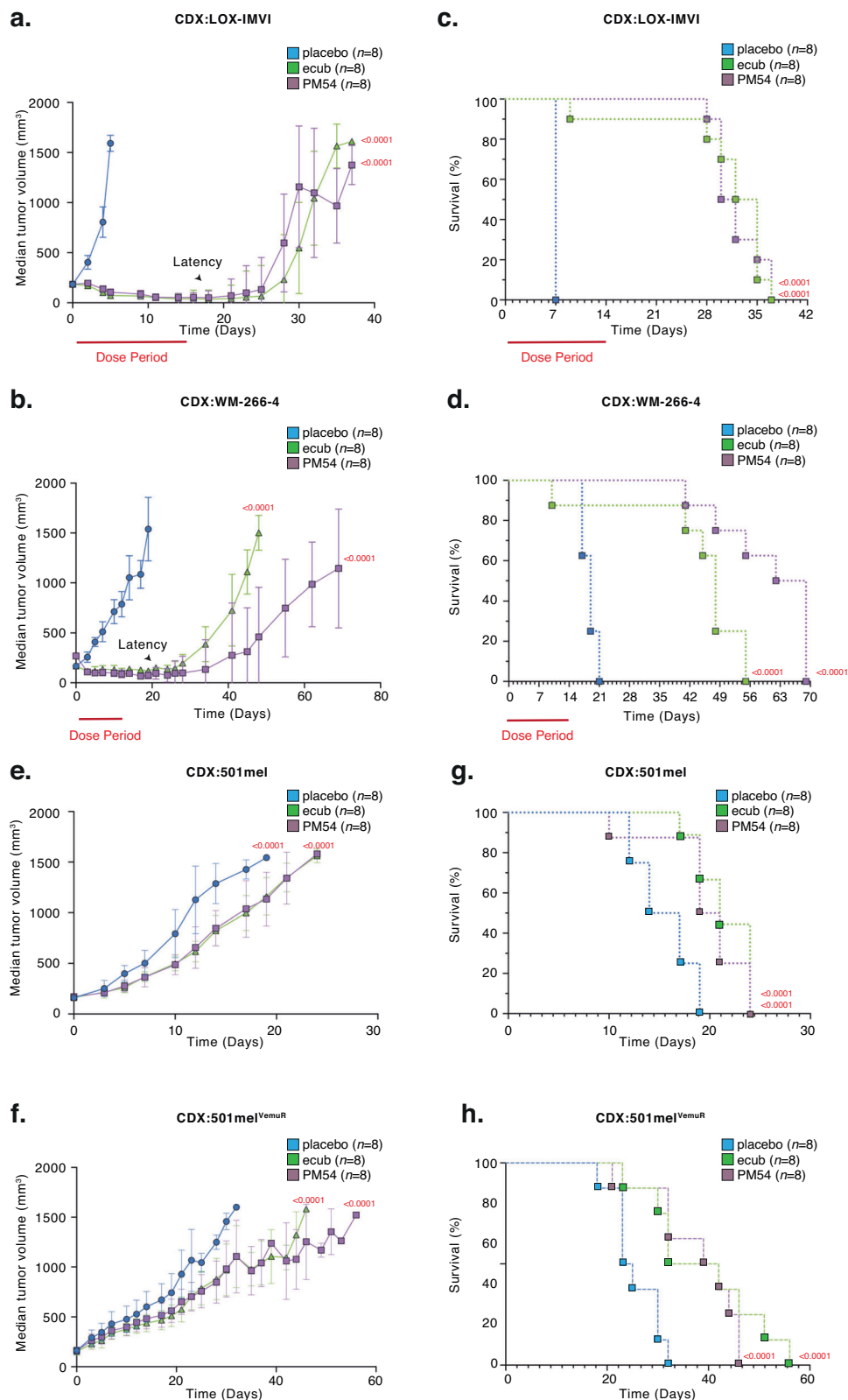
We next undertook a comparative analysis of gene expression profiles in response to treatment with synthetic ecteinascidins. Notably, the three molecules commonly down-regulated 1365 and 1104 genes in differentiated and undifferentiated cells, respectively (Supplementary Fig. 6a). It is worth mentioning that among these genes, 757 displayed consistent down-regulation (and only 110 displayed up-regulation) across both differentiated and undifferentiated cells in response to all the three compounds (Supplementary Fig. 6b,c,d and Supplementary Data 2). Gene ontology (GO) analysis revealed that a substantial proportion of these 757 genes were intricately involved in transcriptional processes (Supplementary Fig. 6e and Supplementary Data 2 and 8).

We subsequently compared each next-generation synthetic ecteinascidin with lurbinectedin. We observed that ecubectedin exhibited strikingly similar effects, with no genes exhibiting statistically significant differential expression upon a comparative analysis in

either differentiated or undifferentiated cells (Supplementary Fig. 7a,b). In stark contrast, PM54 distinctly induced specific transcriptional effects compared to lurbinectedin, revealing a more focused alteration in gene expression, as a smaller subset of genes exhibited deregulation in both differentiated and undifferentiated melanoma cells, (Supplementary Fig. 7a,c). This distinction was further substantiated by GO analysis, which elucidated that PM54 exerts weaker effects on genes involved in diverse cellular processes such as interferon response or oxidative phosphorylation but exerts a more direct influence on genes involved in transcriptional regulation (Supplementary Fig. 7d and Supplementary Data 2 and 8). Globally, our analysis demonstrates that PM54 distinguishes itself by exerting the least influence on the transcriptional program of melanoma cells, while presenting virtually the same cytotoxic effects, emphasizing a unique and potentially advantageous pharmacological profile.

Synthetic ecteinascidins suppress the expression of SE-dependent genes

To decipher the molecular mechanism underlying the cytotoxicity of synthetic ecteinascidins, we conducted an extensive analysis of RNA-Seq datasets derived from three distinct cancer cell types treated with



lurbinectedin. These cells were derived from metastatic melanoma (501mel), metastatic non-SCLC (A549) ([GSE179074](#)³⁵) and metastatic SCLC (DMS53) ([GSE179074](#)³⁵), the latter being a cancer type for which lurbinectedin has recently gained clinical approval. This analysis revealed that a common set of 642 genes underwent significant down-regulation upon drug exposure (Fig. 5a and Supplementary Data 3). GO analysis revealed once again a strong enrichment of genes involved in

transcriptional regulation (Supplementary Fig. 8a and Supplementary Data 2 and 8), with notable downregulated genes including ubiquitous transcription factors/coactivators (such as *CDK7*, *CDK12*, *CDK13*, *E1A-associated cellular p300 (EP300)*, *CREB-binding protein (CBP)*) and genes coding for Mediator complex subunits (such as *CDK8* and *MED13*). These results were confirmed in differentiated and undifferentiated melanoma cells by immunoblotting (Fig. 5b). Notably, in vivo

Fig. 4 | Potent in vivo effects of synthetic ecteinascidins. **a, b** Indicated CDX models ($n = 10$ at the beginning of the experiment) from LOX-IMVI **a** or WM-266-4 **b** melanoma cells were treated with placebo, ecubectedin or PM54 at 1.2 mg/kg once a week for 3 consecutive weeks (on days 0, 7 and 14) and tumor volumes were measured. Results are shown as mean values \pm SD for “ n ” mice. The red bar indicates the dose period. The latency phase is indicated by an arrow. Logrank (Mantel–Cox) test was used to determine the p -values. Source data are provided as a Source Data file. **c, d** Indicated CDX models ($n = 10$ at the beginning of the experiment) from LOX-IMVI **c** or WM-266-4 **d** melanoma cells were treated weekly with Placebo, ecubectedin or PM54 at 1.2 mg/kg and survival was assessed. Results are shown as mean values \pm SD for “ n ” mice. The red bar indicates the dose period. The latency phase is indicated by an arrow. Logrank (Mantel–Cox) test was used

to determine the p -values. Source data are provided as a Source Data file. **e, f** Indicated CDX models ($n = 8$ at the beginning of the experiment) from 501mel **e** or 501mel^{VenuR} **f** melanoma cells were treated once with Placebo, ecubectedin or PM54 at 1.2 mg/kg and tumor volumes were measured. Results are shown as mean values \pm SD for “ n ” mice. Logrank (Mantel–Cox) test was used to determine the p -values. Source data are provided as a Source Data file. **g, h** Indicated CDX models ($n = 8$ at the beginning of the experiment) from 501mel **g** or 501mel^{VenuR} **h** melanoma cells were treated once with Placebo, ecubectedin or PM54 at 1.2 mg/kg and survival was assessed. Results are shown as mean values \pm SD for “ n ” mice. Logrank (Mantel–Cox) test was used to determine the p -values. Source data are provided as a Source Data file.

experiments utilizing melanoma CDXs also demonstrated a rapid down-regulation of these genes, together with lineage-specific master transcription factors such as *MITF*, *SOX10* or *PAX3* following short-term treatments with synthetic ecteinascidins (Fig. 5c).

Ubiquitous transcription factors/coactivators and the mediator complex are pivotal in driving oncogenic expression in cancer cells by activating genes dependent on SEs. Therefore, in an effort to identify SEs in our melanoma cell models, we performed Cut&Tag assays targeting H3K27ac and BRD4 in differentiated and undifferentiated cells (501mel and MM029, respectively). Using the Rank Ordering of Super-Enhancers (ROSE) algorithm and cross-referencing the list of SEs identified from the Cut&Tag on H3K27ac and that on BRD4, we identified 533 and 347 bona fide SEs in differentiated and undifferentiated metastatic melanoma cells, respectively (Supplementary Fig. 8b,c and Supplementary Data 4). Subsequently, we identified by ROSE 1,255 and 951 genes putatively regulated by these bona fide SEs, in differentiated and undifferentiated melanoma cells, respectively (Supplementary Fig. 8d and Supplementary Data 4). Although 261 SE-dependent genes were shared between differentiated and undifferentiated cells, most SE-dependent genes seemed to be cell-state-specific. We next crossed these data with the list of downregulated genes in both differentiated and undifferentiated metastatic melanoma cells following treatments with synthetic ecteinascidins and observed a significant enrichment of SE-dependent genes among those down-regulated genes (Fig. 5d). This was also observed in vivo, where SE-dependent oncogenes such as *MITF*, *SOX10*, *SAMMSON* or *MYC* were strongly downregulated upon treatment with synthetic ecteinascidins (Fig. 5c).

Synthetic ecteinascidins target transcriptionally active, CpG-rich genomic regions

We next sought to map the genome-wide binding sites of synthetic ecteinascidins in melanoma cells. Using bioactive biotinylated versions of lurbinectedin and PM54 (Bio-lurbi and Bio-PM54) (Table 1), we conducted an in situ mapping of our compounds to genomic DNA using Chem-map⁴¹. We performed three biological replicates per compound, using both differentiated or undifferentiated melanoma cells (501mel and MM029, respectively), observing a high reproducibility with Spearman correlations exceeding 0.7 (Supplementary Fig. 9a). Our analysis revealed approximately 30,000 drug-binding sites in differentiated and 15,000 in undifferentiated cells (Fig. 6a and Supplementary Data 5). Notably, approximately 75 % of the identified drug-binding sites were found to be located in gene regions, with promoter (~25–34 %) and intronic (~32–35%) binding frequencies being consistent for both Bio-lurbi and Bio-PM54, in both cell types (Fig. 6b and Supplementary Fig. 9b). Overall, we observed a highly significant correlation between drug-bound gene promoters and genes down-regulated by the drugs (Fig. 6c and Supplementary Fig. 9c). Genome-wide, peaks of synthetic ecteinascidins predominantly co-localized with the transcriptionally active H3K27ac chromatin mark, RNAPII, BRD4 and positive ATAC-seq signals, and not with the repressive H3K27me3 chromatin mark (GSE205463⁴²) (Fig. 6d and Supplementary Fig. 9d). Indeed, between 80 and 90 % of

the synthetic ecteinascidins binding sites in 501mel and MM029 cells exhibited substantial overlaps with ATAC-seq signals (Fig. 6e and Supplementary Fig. 9e–g). Furthermore, our genome-wide analysis indicated that over 35% of synthetic ecteinascidins binding sites in 501mel cells and over 45 % in MM029 cells exhibited substantial overlaps with CpG islands (Fig. 6f and Supplementary Fig. 9h). Most of the CpG islands bound by the drugs were located in open chromatin regions, positive for ATAC-seq signal (Fig. 6g and Supplementary Fig. 9i). These data underscore the preferential binding of synthetic ecteinascidins to transcriptionally active genomic sites such as promoter regions, and suggest that they target the CpG islands located within these sites.

Synthetic ecteinascidins exhibit distinct patterns of chromatin binding associated with cell phenotypes

We subsequently integrated the chem-map data and observed a robust overlap (~80%) between the promoter regions bound by Bio-lurbi and those bound by Bio-PM54 in a given cell type (Fig. 7a, left panel). Notably, among the promoters bound by synthetic ecteinascidins, a significant fraction demonstrated concurrent binding by the two drugs in both cell types (Fig. 7a, right panel). This included promoters that regulate the expression of ubiquitous transcription factors/coactivators or Mediator subunits (Supplementary Data 6). In these promoters, such as those regulating expression of *EP300* or *CDK7*, a pronounced overlap was observed between the binding sites of synthetic ecteinascidins and CpG islands, H3K27ac, RNAPII and ATAC-seq signal (Fig. 7b).

Apart from the commonality in drug-bound promoters depicted above, each melanoma cell type also exhibited a subset of distinct and unique binding sites associated with its specific cellular phenotype. We observed a strong overlap between cell-state-exclusive binding sites and cell-state-specific H3K27ac sites at the corresponding genomic loci, once again suggesting a connection between drug binding and open chromatin (Fig. 7c and Supplementary Fig. 10a–d). In these specific binding sites, we identified sets of promoters which indeed demonstrated exclusive activity in either differentiated or undifferentiated cells. For instance, synthetic ecteinascidins bound to the promoter of the lineage-specific master transcription factor *MITF* gene only in differentiated cells, where it is highly expressed (Fig. 7d). Conversely, the promoter regulating the *Baculoviral IAP repeat-containing protein 3* gene (*BIRC3*), an inhibitor of apoptosis expressed only in undifferentiated melanoma cells, was occupied by synthetic ecteinascidins in undifferentiated but not in differentiated cells (Fig. 7e).

When examining the deposition of synthetic ecteinascidins along the *MITF* gene, drug-binding to its SE was also observed (Fig. 7d). In agreement, almost all (~95 %) of the bona fide SEs identified by ROSE in differentiated and undifferentiated cells were directly bound by the compounds (Fig. 7f). To gain a global understanding of the interplay between synthetic ecteinascidins and enhancer activity, we used the Active-By-Contact (ABC) model⁴³ to integrate our ATAC-seq, Cut&Tag, and RNAseq data with publicly available HiC data obtained in

differentiated melanoma cells (GSE105491⁴⁴). We generated a genome-wide annotation of all active cis-candidate regulatory regions (cCRE) directly implicated in activating gene expression in 501mel cells

(Supplementary Fig. 11a). Based on differential gene expression data, this model thus allowed the prediction of interactions between active enhancers and genes that were either positively or negatively

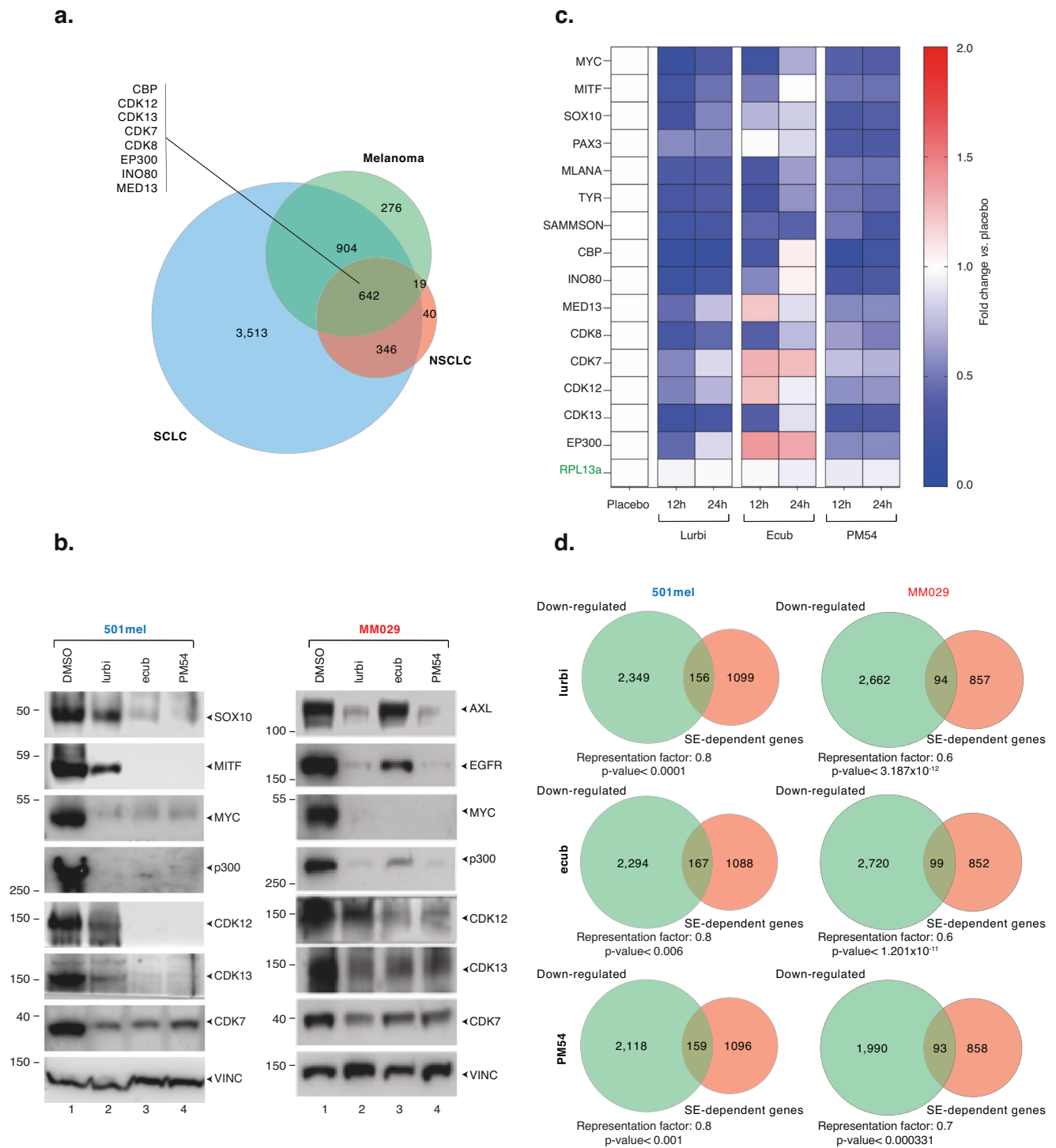
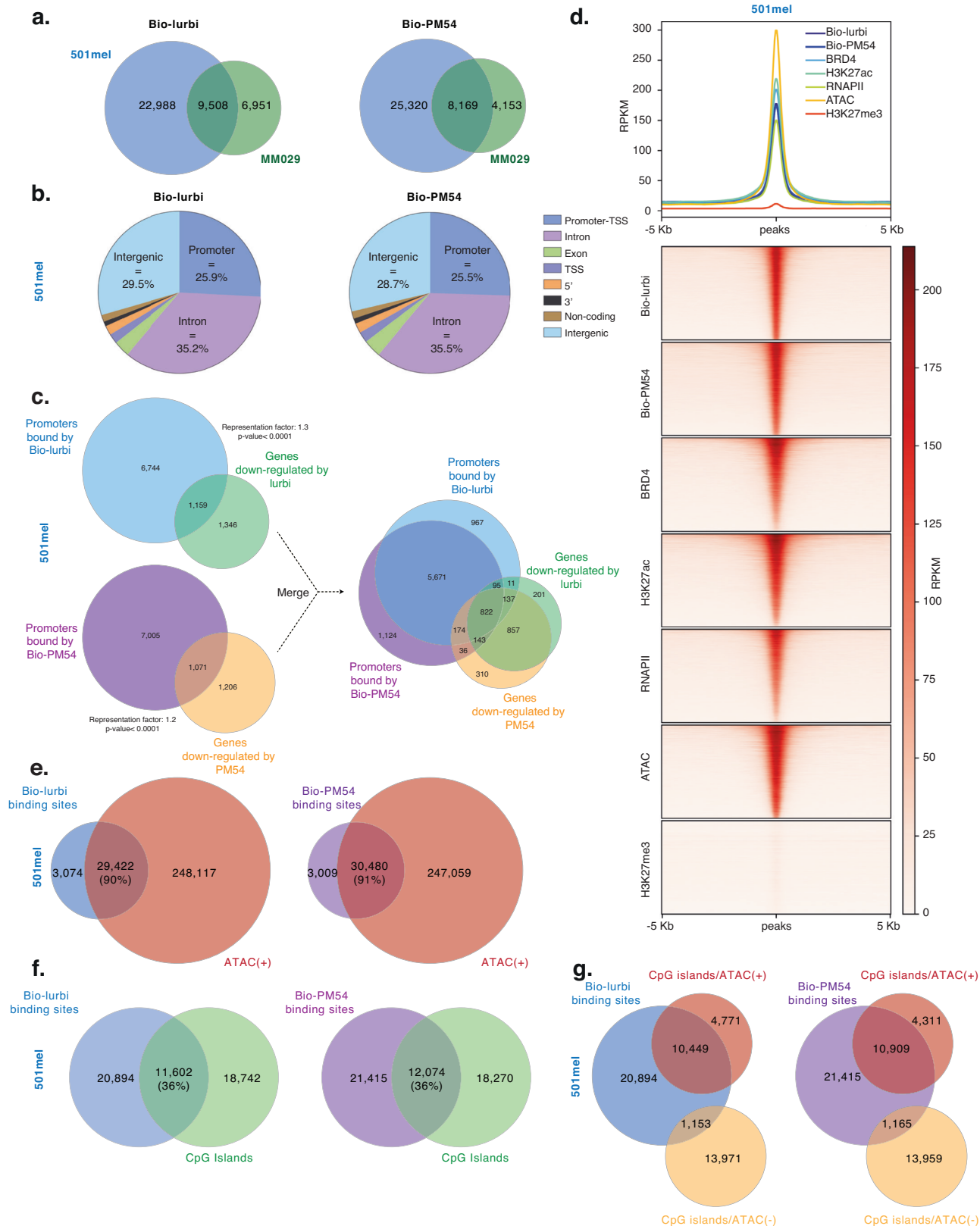


Fig. 5 | Synthetic ecteinascidins inhibit the expression of SE-dependent genes. **a** Venn diagram showing the overlap of genes down-regulated in melanoma (GSE256100), SCLC (GSE179074) and NSCLC (GSE179074), following treatment with lurbinectedin. **b** Differentiated 501mel (left) or undifferentiated MM029 (right) melanoma cells were treated with synthetic ecteinascidins as indicated (5xIC50 concentration, 24 h) and protein lysates were immuno-blotted for proteins as indicated. Molecular mass of the proteins is indicated (kDa). Source data are provided as a Source Data file. This experiment was repeated independently three times with similar results. **c** CDXs from 501mel cells ($n = 3$) were treated with a single dose of

lurbinectedin, ecubectedin or PM54 at 1.2 mg/kg and tumors were collected 12 or 24 h later. Heatmap shows average placebo-normalized expression of the indicated genes obtained by qRT-PCR analysis. RPL13a is a housekeeping gene. **d** Venn diagram showing the overlap of genes down-regulated by synthetic ecteinascidins, as indicated, in 501mel (left) or MM029 cells (right) (10xIC50 concentration, 8 h) ($n = 3$) and SE-dependent genes identified in these cells using H3K27ac- and BRD4-profiling by Cut&Tag and the ROSE algorithm⁴². Representation factor and hypergeometric p -value are indicated and were determined using Graeber lab software. Hypergeometric distribution test was used to determine the p -values.



impacted by treatment with synthetic ecteinascidins. Notably, 4436 enhancers were inferred to be in contact with the promoters of genes down-regulated by treatment with synthetic ecteinascidins, such as the SE controlling SOX10 expression (Supplementary Fig. 11b), while only 736 enhancers were inferred to be in contact with promoters of genes up-regulated by the same treatments (Supplementary Data 6). Enhancers controlling the expression of down-regulated genes tended

to be characterized by a higher ABC-score (higher enhancer activity) and contacted more genes than enhancers controlling expression of up-regulated genes (Supplementary Fig. 11c). In conclusion, the ABC model indicates that genes under the dependence of strong enhancers, such as SEs, might be particularly vulnerable to synthetic ecteinascidins, and that active enhancer-promoter interactions might be weakened by drug binding.

Fig. 6 | Synthetic ecteinascidins bind to CpG-rich sequences located in open chromatin regions. **a** Venn diagram of drug-binding sites (Bio-lurbi in the left and Bio-PM54 in the right) in 501mel vs. MMO29 cells ($n = 3$). **b** Pie chart showing the distribution of annotated peaks (in percentages) for Bio-lurbi (top) and Bio-PM54 (bottom) all over the genome (hg19) in 501mel cells ($n = 3$). **c** Left panel: Venn diagram ($n = 3$) between promoters bound by Bio-lurbi or Bio-PM54 and genes down-regulated by lurbinectedin or PM54 in 501mel cells. Right panel: the two Venn diagrams ($n = 3$) were merged. Representation factor and hypergeometric p -value are indicated and were determined using Graeber lab software. Hypergeometric distribution test was used to determine the p -values. **d** Upper panel: Metaplot distribution ($n = 3$) of Bio-lurbi, Bio-PM54, BRD4, RNAPII, H3K27ac, H3K27me3 enrichment and ATAC-Seq signals in a ± 5 kb window around the occupied DNA binding sites of Bio-lurbi in differentiated 501mel cells. Lower panel: Heatmap

profiles representing the read density clusterings obtained with seqMINER for the DNA-occupied sites of Bio-lurbi in differentiated 501mel cells relative to Bio-PM54, BRD4, RNAPII, H3K27ac, H3K27me3 enrichments and ATAC-Seq signals. Peak order is determined by Bio-lurbi and identical for all clusterings. **e** Venn diagram ($n = 3$) between Bio-lurbi (left) or Bio-PM54 (right) binding sites and positive ATAC-seq peaks (indicative of chromatin open regions) in differentiated 501mel cells. **f** Venn diagram ($n = 3$) between Bio-lurbi (left) or Bio-PM54 (right) binding sites and human CpG islands in differentiated 501mel cells. **g** Venn diagram ($n = 3$) between Bio-lurbi (left) and Bio-PM54 (right) binding sites in differentiated 501mel cells and human CpG islands. Human CpG islands are divided into those found in open chromatin regions (CpG islands/ATAC(+)) and those found in closed chromatin regions (CpG islands/ATAC(-)).

Collectively, these findings suggest that synthetic ecteinascidins impact SE-mediated oncogenic transcription by binding to and inhibiting the activity of the promoters of ubiquitous transcription factors/coactivators enriched at SEs, and potentially by directly targeting the enhancer/SEs driving oncogenic expression.

Synthetic ecteinascidins disrupt coactivator condensation at SEs

It was demonstrated that SE-enriched transcriptional coactivators such as BRD4 or the MED1 subunit of the Mediator complex form discrete nuclear puncta at SEs *ex vivo* to ensure robust expression of SE-dependent genes⁹. Based on the above data, we hypothesized that synthetic ecteinascidins could disrupt these condensates. Immunofluorescence revealed nuclear puncta for BRD4 that co-localized with the SE-specific histone mark H3K27ac in differentiated or undifferentiated melanoma cells (Supplementary Fig. 12a). Synthetic ecteinascidins disrupted BRD4 and MED1 puncta in both types of cells, similar to what was observed with 1,6-hexanediol, widely used to disorganize liquid-like condensates⁹ (Fig. 8a, b and Supplementary Fig. 12b). In contrast, treatment with dacarbazine, an alkylating compound that causes DNA damage and that is clinically used in the treatment of melanoma, did not affect BRD4 and MED1 puncta (Fig. 8a, b and Supplementary Fig. 12b). Treatment with the MEKi trametinib even resulted in a significant increase in BRD4 and MED1 puncta, likely due to the reprogramming of enhancer/SE formation observed in melanoma cells following MEKi treatment, leading to hyperdifferentiation⁴⁵. In agreement with these observations, trametinib and dacarbazine did not decrease the expression of SE-dependent genes such as *MITF* and *SOX10* in differentiated cells (MEKi even increased their expression) or *AXL* and *EGFR* in undifferentiated cells (Supplementary Fig. 12c,d). ChIP-qPCR was used to further reveal that together with the inhibition of expression observed above, the level of H3K27ac and BRD4 was significantly reduced at the SEs regulating the expression of *MITF*, *SOX10*, *EGFR* or *AXL*, upon short-term treatment with synthetic ecteinascidins (Fig. 8c, d and Supplementary Fig. 12e,f). Note also that the level of H3K27ac was unaffected at the promoter of the 60S Ribosomal Protein L13a (*RPL13a*) housekeeping gene in these conditions (Supplementary Fig. 12g,h). Collectively, these results indicate that synthetic ecteinascidins disrupt the integrity of transcriptional condensates, consequently leading to the inactivation of SEs. They also highlight the specific mechanism of action of these drugs compared to current clinical treatments.

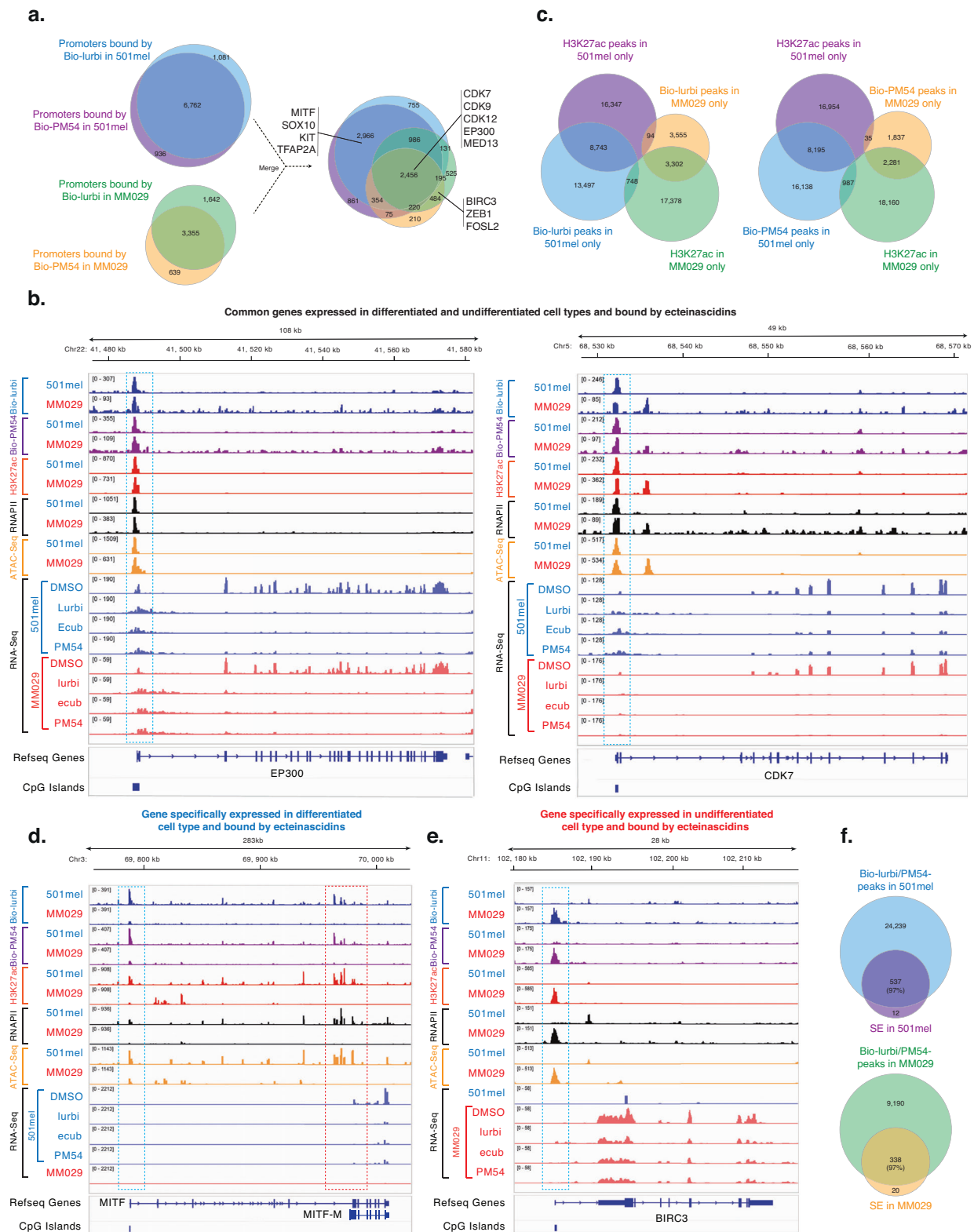
Synthetic ecteinascidins induce waves of transcriptional inhibition in melanoma and SCLC cells

The data above imply a model in which the inhibition of ubiquitous transcription factors/coactivators induces the inhibition of SE-dependent oncogenes. To test this model, we conducted kinetic analyzes, revealing that transcription factors/coactivators were down-regulated before SE-dependent genes in melanoma cells (Fig. 9a, b and Supplementary Fig. 13a,b). We explored whether a similar mechanism

could occur in SCLC following treatment with synthetic ecteinascidins. We observed that transcription factors/coactivators were down-regulated very early in SCLC DMS53 cells upon treatments with synthetic ecteinascidins, followed by the inhibition of SCLC-specific SE-dependent genes such as *Achaete-scute homolog 1 (ASCL1)*, *B-Cell Leukemia/Lymphoma 2 (BCL2)*, *MYC*, *Neurogenic Differentiation Factor 1 (NEUROD1)* or *TEAD1* genes (Fig. 9c). In agreement, a significant enrichment of SE-dependent genes was observed among those down-regulated upon treatment with synthetic ecteinascidins in these cells (Supplementary Fig. 13c). While the ChIP-qPCR data in Fig. 8 cannot be generalized to all dysregulated genes in melanoma, we extended this analysis to SCLC using published data (GSE179074³⁵). We re-analyzed these data by focusing on three groups of genes with H3K27ac peaks at their TSS: those commonly down-regulated in melanoma, SCLC, and NCLC (348 genes); SCLC-specific SE-dependent genes (424 genes); and genes that were commonly unaffected (1434 genes) (Supplementary Data 7). ChIP-seq for H3K27ac, performed before and after treatment with lurbinectedin (GSE195663³⁵), revealed a loss of this active transcriptional mark at the promoters of commonly down-regulated genes (e.g., *CDK8*) and SCLC-specific super-enhancer-dependent genes (e.g., *MYC*) (Fig. 9d, e). Notably, H3K27ac was significantly less affected at the promoters of genes whose expression was unaffected by lurbinectedin, such as the housekeeping gene *RPL13a*. Overall, these data suggest that synthetic ecteinascidins induce an initial inactivation of promoters regulating the expression of transcription factors and coactivators, which triggers a secondary inactivation of the promoters of SE-dependent oncogenes.

Discussion

Metastatic melanoma cells exhibit significantly higher mutational burdens compared to other cancer types, potentially leading to proportional dysregulation of gene expression patterns. Furthermore, the well-documented cell-state plasticity of melanoma cells underscores their robust reliance on tightly regulated oncogenic gene expression programs. This cancer type, therefore, serves as an ideal model for investigating the clinical relevance and therapeutic potential of targeting oncogenic transcriptional addiction. Comparative analyzes were conducted to evaluate the impact of three synthetic ecteinascidins relative to clinically utilized MAPKi agents. Notably, metastatic undifferentiated melanoma cells displaying inherent resistance to MAPKi/immunotherapy, as well as *in vitro* engineered hyperpigmented cells with acquired MAPKi resistance¹⁴, exhibited comparable sensitivity to the three synthetic ecteinascidins at low nanomolar concentrations. Single-cell sequencing has unveiled additional cell states within melanoma tumors, such as interferon-active melanoma cells that emerge during the minimal residual disease phase, post-treatment with MAPKi^{19,30}. The significance of these cells in the context of resistance to treatment has been significantly underestimated. In an attempt to mimic these cell subpopulations *in vitro*, we have generated pseudo-interferon-active melanoma cells by treatment with interferon- γ . Intriguingly, these pseudo-interferon-active melanoma



cells exhibited sustained sensitivity to synthetic ecteinascidins while acquiring resistance to MAPKi (Supplementary Fig. 14 and Table 1). In vivo, we observed significant decreases in mitotic indexes and increases in cell death and overall survival in four different melanoma CDX models, including MAPKi-resistant CDXs. Our data demonstrate that synthetic ecteinascidins exhibit high cytotoxic impact both in vitro and in vivo on the most common melanoma cell phenotypes, as

well as on drug-tolerant cell populations emerging during the minimal residual disease phase.

Our results elucidate the mechanisms of action of synthetic ecteinascidins, highlighting their common features and revealing some notable differential molecular effects. Low nanomolar doses of synthetic ecteinascidins consistently reduced the proliferation and invasive capacities of metastatic melanoma cells while inducing

Fig. 7 | Synthetic ecteinascidins exhibit distinct patterns of chromatin binding associated with cell phenotypes. **a** Left panel: Venn diagrams ($n = 3$) between promoters bound by Bio-lurbi and Bio-PM54 in 501mel (top) and MM029 (bottom) cells. Right panel: the two Venn diagrams were merged. **b** Gene tracks of Bio-lurbi, Bio-PM54, RNAPII, H3K27ac occupancy, ATAC-seq and RNA-Seq signals at CDK7 (left) or EP300 (right) loci in 501mel or MM029 cells. RNA-Seq signals show that these genes are expressed in both 501mel and MM029 melanoma cells. In blue, drug binding at promoters is highlighted. Localization of CpG islands is shown. **c** Left panel: Venn diagrams ($n = 3$) comparing genomic bindings sites uniquely bound by Bio-lurbi in either 501mel or MM029 cells with H3K27ac peaks found exclusively in either 501mel or MM029 cells. Right panel: Venn diagrams comparing genomic bindings sites uniquely bound by Bio-PM54 in either 501mel or MM029 cells with H3K27ac peaks found exclusively in either 501mel or MM029 cells. We considered different peaks as overlapping if there was at least 1 bp of overlap. **d** Gene tracks of Bio-lurbi, Bio-PM54, RNAPII, H3K27ac occupancy, ATAC-seq and

RNA-Seq signals at the MITF locus in 501mel or MM029 cells. RNA-Seq signals show that this gene is only expressed in differentiated 501mel cells. The red square indicates the SE regulating the expression of MITF. In blue, drug binding at the promoter is highlighted. In red, drug binding at the SE is highlighted. Localization of CpG islands is shown. Note that MITF-M isoform is expressed in melanoma. **e** Gene tracks of Bio-lurbi, Bio-PM54, RNAPII, H3K27ac occupancy, ATAC-Seq and RNA-Seq signals at the BIRC3 locus in 501mel or MM029 cells. RNA-Seq signals show that this gene is only expressed in undifferentiated MM029 melanoma cells. In blue, drug binding at the promoter is highlighted. Localization of CpG islands is shown. **f** Upper panel: Venn diagrams ($n = 3$) comparing all genomic bindings sites commonly bound by Bio-lurbi and Bio-PM54 and bona fide super-enhancers identified in 501mel cells. Lower panel: Venn diagrams comparing all genomic bindings sites commonly bound by Bio-lurbi and Bio-PM54 and bona fide super-enhancers identified in MM029 cells.

apoptosis and blocking the cell cycle in the G2/M phase. Drug treatments also led to the significant disruption of oncogene expression. Importantly, the transcriptional effects of the compounds appeared to exhibit a high degree of specificity for distinctly overexpressed oncogenes depending on the melanoma cell state. For instance, while the expression of housekeeping genes was unaffected in 2- or 3-D conditions by short-term drug treatments, lineage-specific drivers of proliferation such as MITF, SOX10 or PAX3 were strongly inhibited specifically in differentiated cells. In undifferentiated cells, different genes were affected, such as the key regulators AXL or EGFR, the anti-apoptotic protein BIRC3 or the cell-type master transcription factors FOSL2 and TEAD4. These observations arguably reveal the most interesting feature of these next-generation compounds: synthetic ecteinascidins appear to specifically inhibit the distinct oncogenic transcription programs on which a given cancer cell subpopulation depends. Thus, this unique mechanism of action differentiates synthetic ecteinascidins from conventional chemotherapeutic DNA-binders/DNA-modifiers, such as platinum derivatives or dacarbazine, which induce DNA damage uniformly across the genome. Moreover, the efficacy of synthetic ecteinascidins does not depend on the phenotypic nature of the melanoma cell, a feature that differentiates these drugs from conventional MAPKi therapies and immunotherapies²⁰.

Mechanistically, our results highlight a multifaceted mechanism of action by which synthetic ecteinascidins impede oncogenic transcription. Synthetic ecteinascidins bind to promoter/enhancer regions of genes encoding ubiquitous transcription factors/coactivators, usually strongly enriched at SEs, leading to their rapid inhibition. This effect is likely potentiated by the fact that promoters/enhancers of genes encoding lineage-specific master transcription factors such as MITF or SOX10 are also heavily bound by synthetic ecteinascidins in melanoma cells. These master regulators are known to bind SEs to form autoregulatory loops that constitute the core transcriptional regulatory circuitries of cancer cells. The disruption of these oncogenic expression loops, coupled with the strong binding of synthetic ecteinascidins to SEs themselves, albeit with uncertain biological consequences, potentially ensures the robust inhibition of SE-driven oncogenic transcription. Importantly, these observations extend beyond melanoma cells, as SE-driven transcription was also inhibited in SCLC cells exposed to synthetic ecteinascidins, establishing these molecules as potential universal pan-disruptors of SEs. Overall, the inhibition of SE-driven oncogenic transcription has a potent cytostatic/cytotoxic impact on cancer cells, as demonstrated in vivo by the inhibition of cell proliferation and induction of apoptosis. In a second line of attack, synthetic ecteinascidins induce DNA breaks that persist over time and that synergize with transcription inhibition to trigger cell death.

Delving deeper into the transcriptional effects elicited by the three compounds, we observed that while the gene expression changes elicited by lurbinectedin and ecubectedin greatly overlapped, the

transcriptional effects of PM54 significantly diverged. Notably, PM54 treatments deregulated fewer genes than lurbinectedin or ecubectedin while eliciting the same cytostatic and cytotoxic effects, potentially representing a clinical benefit. Although the exact mechanism explaining this difference is yet to be determined, it may be related to the fact that the moiety modified in PM54 vs. lurbinectedin is located in the area of the molecule described as interacting with DNA binding proteins/transcription factors⁴⁶. Such a differential interaction between the drug and transcription factors might result in fewer systemic gene expression disruptions and, thus, fewer unwanted secondary effects, while still potently targeting oncogenic SE-dependent gene expression, leading to cancer cell death. Consequently, Phase I clinical trials for PM54 in advanced solid tumors, including melanoma, were initiated (ClinicalTrials.gov Identifier: NCT05841563, EudraCT Number 2022-002031-65).

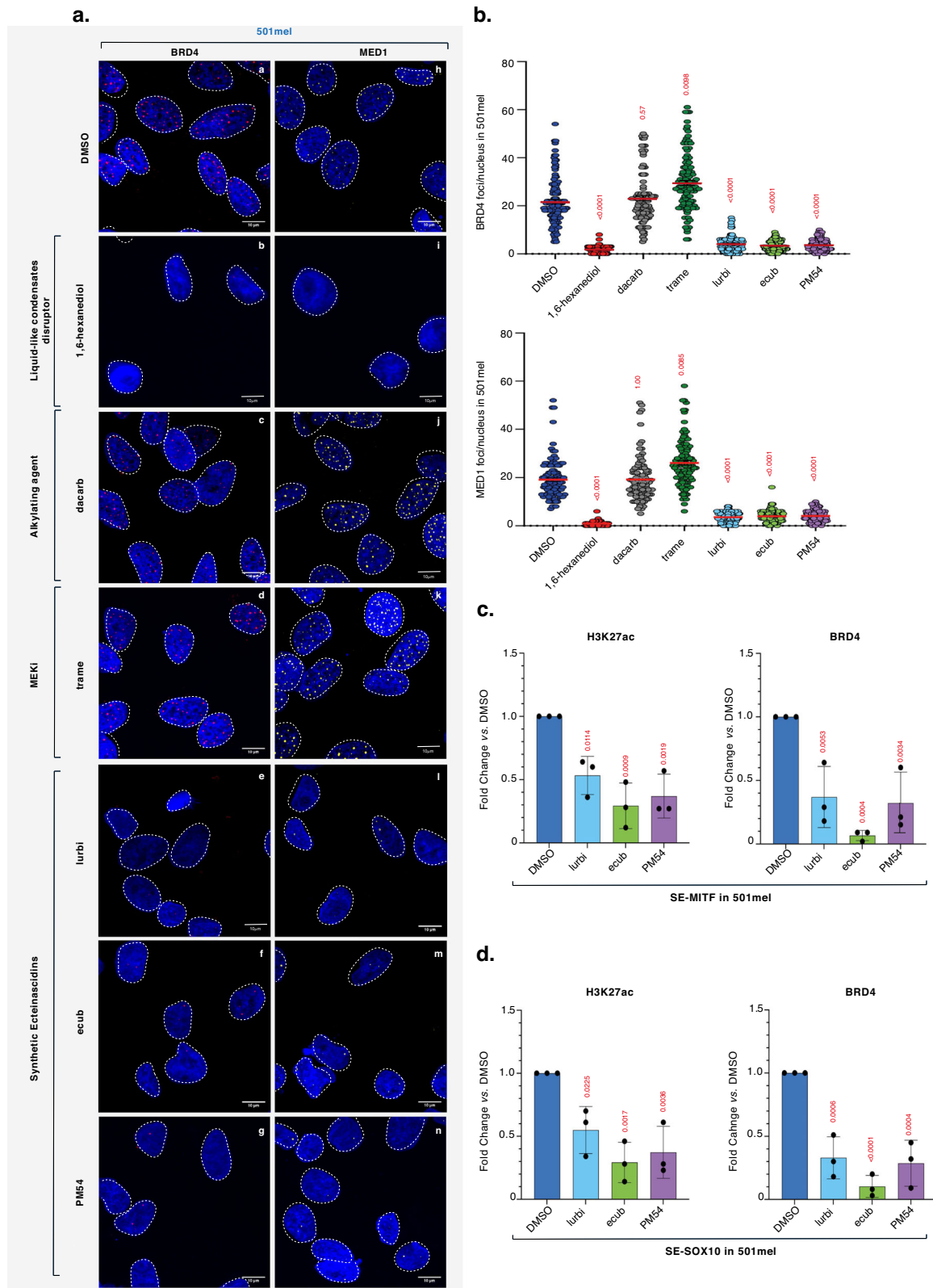
Collectively, our data provide a comprehensive overview of the cellular and molecular effects of a potential therapeutic approach to melanoma and other transcriptionally-addicted cancers based on SE-dependent oncogenic inhibition. The current study further illuminates the intricacies of gene expression dependencies of different melanoma cell subpopulations and their molecular responses to transcriptional disruptions. This preclinical work might justify the clinical testing of synthetic ecteinascidins as a second-line melanoma treatment following MAPKi/immunotherapy relapse, but it also highlights the potential benefits of further exploring the effects of additional structural analogs. Finally, recent observations demonstrated that synthetic ecteinascidins, such as lurbinectedin, synergize with immune checkpoint blockade and stimulates proliferation of CD4+ and CD8+ T cells. These immune-modulatory functions make synthetic ecteinascidins a potential platform for immunotherapy combination in melanoma^{47,48}.

Methods

All animal experimental procedures were reviewed and approved by an Internal Ethical Committee and by “O.H. Universidad Miguel Hernandez de Elche” and “O.H. Hospital General Universitario Gregorio Marañón”, and, finally, authorized by “Comunidad Autónoma de Madrid, CAM” (regional Institutional Animal Care and Use Committee), reference PROEX 042/16 and PROEX 285.7/23. All experimental procedures were performed in accordance with national and international laws and policies: Spanish directive RD 53/2013 and EU Directive 2010/63/EU. Animals were euthanized through the administration of an overdose of a general anesthetic when their tumors reached ca. 1500 mm³ and/or severe necrosis was seen. Treatments which produced >20 % lethality and/or 20 % net body weight loss were considered toxic and stopped.

Cell culture and treatment

When registered, cells used in this work are identified by a research resource identification number (RRID number (<https://rrid.site>)). Cell



line identity, when applicable, was confirmed annually through STR profiling provided by ATCC's cell authentication service. Hermes3A, RRID:CVCL_VS10; DMS53, RRID:CVCL_1177; 501mel, RRID:CVCL_4633; SKMEL-28, RRID:CVCL_0526; IGR37, RRID:CVCL_2075; IGR39, RRID:CVCL_2076; WM266-4, RRID:CVCL_2765; LOX-IMVI, RRID:CVCL_1381; A549, RRID:CVCL_0023; HaCaT, RRID:CVCL_0038; MRC5, RRID:CVCL_0440. All cells were obtained from ATCC or

collaborators, as indicated in Supplementary Data 8. Cells were grown at 37 °C in 5% CO₂ (10 % for Hermes 3A) and were regularly checked for mycoplasma contamination by the PluriCell East Platform (<https://www.igbmc.fr/en/plateforms-and-services/pluricell-east>). MM patient-derived short-term melanoma cultures (MM011, MM074, MM117, MM029, MM047, MM099) are derived from patient biopsies and were grown in HAM-F10 (Gibco, Invitrogen) supplemented with 10

Fig. 8 | Synthetic ecteinascidins disrupt transcription factor/coactivator condensates at SEs. **a** Representative confocal microscopy images ($n = 3$) of 501mel melanoma cells treated with either DMSO, the condensate disruptor 1,6-hexanediol (3% vol, 20 min), the MEKi trametinib (15 nM, 10 h), the DNA damaging agent dacarbazine (50 μ M, 10 h) or the synthetic ecteinascidins (5xIC50, 10 h). Cells were immunostained with anti-BRD4 (red) or anti-MED1 (white) antibodies. Images of the cells were obtained with the same microscopy system and constant acquisition parameters for a given staining. Source data are provided as a Source Data file. Scale bar: 10 μ m. **b** The numbers of MED1 and BRD4 foci per nucleus observed in 501mel

cells following treatment with the drugs described above are shown \pm SD for three biological triplicates. Red bars indicate mean integrated density. One-way ANOVA with post-hoc Tukey adjustment comparisons were used to determine the p -values (vs. DMSO). **c, d** ChIP-qPCR monitoring the fold change of H3K27ac mark or BRD4 protein at the SEs regulating MITF (left) or SOX10 (right) in mock- or synthetic ecteinascidin-treated (5xIC50, 10 h) differentiated 501mel cells. Error bars indicate mean values \pm SD for three biological triplicates. One-way ANOVA with post-hoc Tukey adjustment comparisons were used to determine the p -values (vs. DMSO). Source data are provided as a Source Data file.

% Fetal Calf Serum (FCS), 25 mM HEPES, 5.2 mM GLUTAMAX and penicillin–streptomycin. Melanoma cell lines 501mel and SKmel28 were grown in RPMI w/o HEPES (Gibco, Invitrogen) supplemented with 10 % FCS and gentamycin. Vemurafenib-resistant cells (501mel^{Vemur} and MM074^{Vemur}) were additionally supplemented with 1.5 mM of vemurafenib. Melanoma IGR cell lines (IGR37 and IGR39) were grown in RPMI w/o HEPES (Gibco, Invitrogen) supplemented with 15 % FCS and gentamycin. Immortalized melanocytes Hermes-3A were grown in RPMI w/o HEPES supplemented with 10 % FCS, penicillin-streptomycin, 200 nM TPA (Sigma Aldrich), 200 p.m. Cholera Toxin (Sigma Aldrich), 10 ng/mL hSCF (Life Technologies), 10 nM EDN-1 (Sigma Aldrich) and 2 mM Glutamine (Invitrogen). HaCaT and MRC5 were grown in DMEM (1g/L glucose) +10% FCS + Gentamycin 40 mg/ml. SCLC cell line DMS53 was grown in Waymouth's MB medium (Gibco, Invitrogen), supplemented with 10% FCS and gentamycin. 501mel, SKmel28, IGR and DMS53 cells were purchased from ATCC, MM and Hermes-3A cells were obtained from collaborators. Vemurafenib (PLX4032), trametinib (GSK1120212), dabrafenib (GSK2118436) and dacarbazine (S1221) were purchased from Selleckchem. 1,6-Hexanediol was obtained from Sigma Aldrich (88571). Lurbinedin (PM1183), ecubectedin (PM14), and PM54 were obtained from PharmaMar S.A. Recombinant Human IFN- γ was obtained from Peprotech (300-02).

Different in vitro drug incubation periods were chosen depending on the nature of the experiments, considering that cell viability is reduced by 50% after 72 h of treatment with 1xIC50 concentrations. For assays studying the impact of the treatments on cancer cell phenotypes related to cancer cell death, such as the inhibition of cell proliferation, the induction of apoptosis and cell cycle blockage, we opted to refer to these same conditions (1xIC50, 72 h). To assess effects preceding cell death, such as impacts on clonogenicity and invasive capacities, a shorter incubation period was chosen (1xIC50, 48 h). For effects relating to gene expression, shorter incubation periods with higher drug concentrations (5xIC50, 12 h for RT-qPCRs; 10xIC50, 8 h for RNA-Seq and Chem-Map, 5xIC50, 24 h for Western Blotting and 5xIC50, 10 h for immunofluorescence and ChIP-qPCR) allowed us to study more closely the immediate and direct effects of the drugs on cancer cell transcriptomes and epigenomes. The used drug concentrations and treatment durations are stated in the respective figure legends.

Protein extraction and western blotting

For whole cell extracts, cells were rinsed once with cold PBS, before pelleting and resuspension in LSDB 0.5 M buffer (500 mM KCl, 50 mM Tris pH 7.9, 20% glycerol, 1% NP-40, 1 mM DTT, phosphatase inhibitor and protease inhibitor cocktail). Afterwards, cells were fully disrupted with 3 cycles of heat shock (liquid nitrogen followed by 37 °C water bath). Then, samples were centrifugated for 15 min at 11,000 g to remove cell debris. Lysates were subjected to SDS–polyacrylamide gel electrophoresis (SDS-PAGE) and proteins were transferred onto a nitrocellulose membrane. Membranes were incubated overnight 4 °C with primary antibodies in PBS + 5% milk powder + 0.01 % Tween-20. The membranes were then incubated with HRP-conjugated secondary antibody (Jackson ImmunoResearch) for 1 h at room temperature and visualized using the ECL detection system (GE Healthcare).

IC50 estimation

Cells were seeded at 5×10^3 cells/well in 96-well plates and treated with increasing concentrations of vemurafenib, dabrafenib, trametinib, lurbinedin, ecubectedin, or PM54. After 72 h of incubation, cells were treated with PrestoBlue reagent (ThermoFisher) according to the manufacturer's instructions. The absorbance per well was measured with a CellInsight CX5 microplate reader (ThermoFisher). Determination of IC50 values was performed by nonlinear curve fitting using the Prism9 statistical software (GraphPad). To assess the effect of IFN γ on drug sensitivities, cells were pre-treated with IFN γ (20 ng/mL) for 24 h, before being treated as mentioned above, while maintaining IFN γ (20 ng/mL) in the medium.

Clonogenicity assay

Cells were drug-treated at IC50 concentrations during 48 h before seeding 1×10^3 or 2×10^3 cells in 6-well plates without drugs, where they grew for 10 days to allow for colony formation. Afterwards, cells were washed once with PBS, then fixed for 10 min with 4% Paraformaldehyde solution, and stained with Crystal Violet solution 0.2% for 15 min. The wells were finally washed twice with deionized water, air dried, scanned and analyzed with Fiji software to count the number of colonies.

Cell proliferation, apoptosis, and cell cycle analysis by flow cytometry

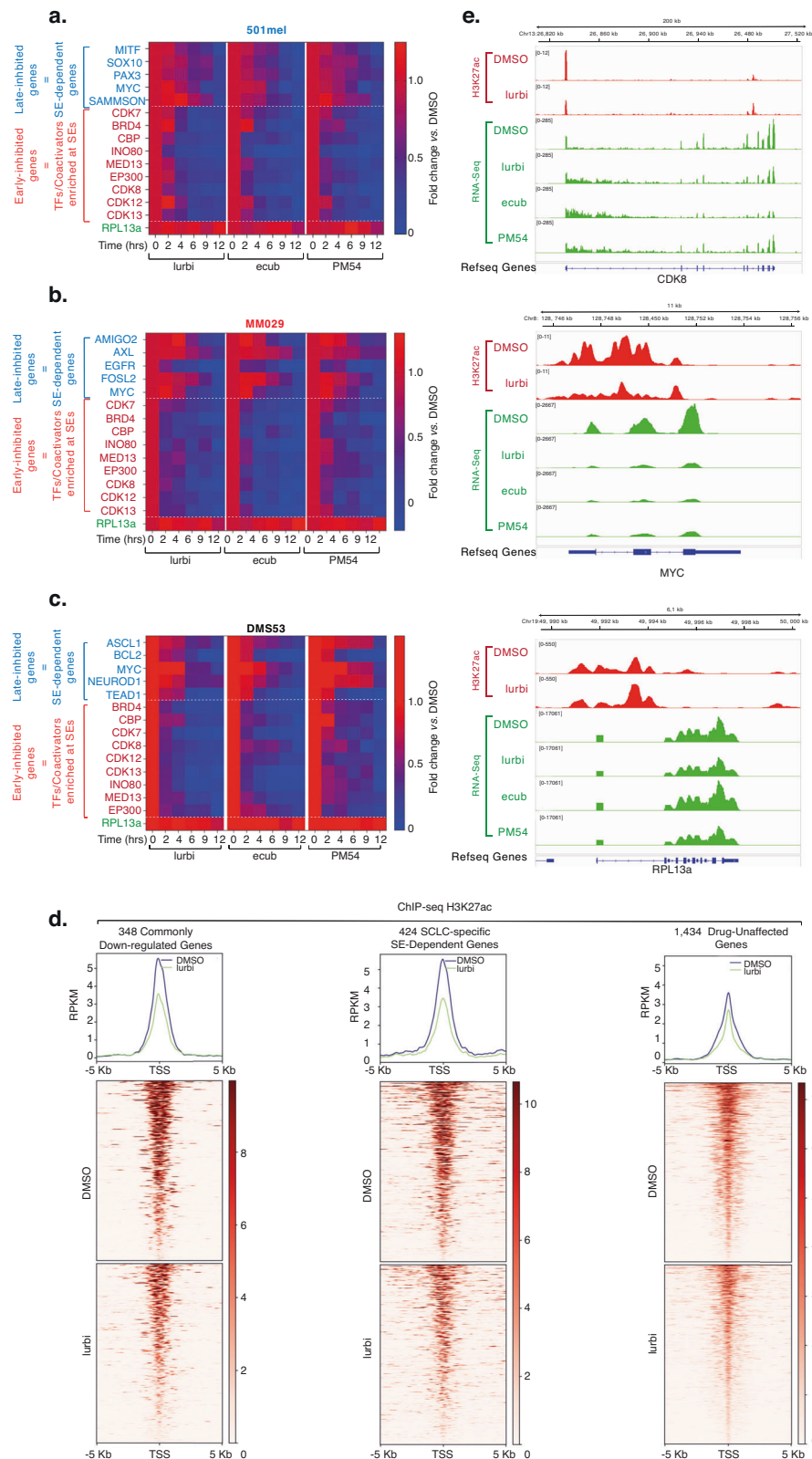
2×10^5 cells were seeded in 6-well plates and were incubated 24 h later with 1 μ M of CellTrace Violet reagent (ThermoFisher) according to the manufacturer's instructions, immediately before rinsing and drug treatment at IC50 concentrations. After 72 h of incubation, cells were rinsed and incubated with AnnexinV-APC (BD Biosciences). Cell proliferation and apoptosis were detected on a BD LSRFortessaTM Flow Cytometer. Data were analyzed with FlowJo software. To define slow proliferating or apoptotic cells, we proceeded as follows: We considered that slow proliferating cells represented the 30 % of cells with the highest concentration of CellTrace Violet signal in the DMSO control. We then calculated the % of cells that had a signal greater than or equal to this value with drug treatment. For apoptotic cells, we considered the 20% of cells with the highest signal of AnnexinV-APC in the DMSO control.

For cell cycle analysis, 2×10^5 cells were seeded in 6 well plates. After 72 h of drug treatments at IC50 concentrations, cells were pelleted and fixed with 70% ethanol for 1 h at 4 °C. After 2 washes with cold PBS, cells were incubated with RNaseA and Propidium Iodide (PI, Biolegend) for 1 h in the dark, before being analyzed on a BD LSRFortessaTM Flow Cytometer. Data were analyzed with FlowJo software.

For apoptosis assays with 3D-grown melanoma cells, TrypLe Select 10x reagent (Gibco) was used to dissociate melanospheres to obtain single-cell suspensions. These cells were incubated with AnnexinV-APC (Biolegend) and PI. With bivariate dot plots, we distinguished between viable (AnnexinV- / PI-), early apoptotic (AnnexinV+ / PI-), late apoptotic (AnnexinV+ / PI+) and necrotic cells (AnnexinV- / PI+).

Boyden chamber invasion assay

2×10^5 cells were seeded inside Boyden Chamber inserts (Fisher Scientific) with 4% Matrigel (Corning) and covered with serum-free media.



The inserts were placed in 24 well plates filled with complete medium. After 24 h, the inserts were washed once with PBS, fixed for 10 min with 4% paraformaldehyde solution, and stained with Crystal Violet solution 0.2% for 15 min. The wells were finally washed twice with deionized water, air dried, and photos were collected using an EVOS xl Core microscope. The pictures were analyzed with Fiji to assess the area of occupancy of the cells.

Melanosphere formation and viability assay

5×10^4 cells were seeded in ultra-low attachment hydrogel-layered 96 well plates in KO DMEM medium supplemented with 20 % KSR, AANE, 2 mM Glutamax, Penicillin/Streptomycin and 100 μ M Beta-mercaptoethanol. To allow for melanosphere formation, cells were left to grow for 4 days before drug treatment.

Fig. 9 | Transcriptional inhibition waves induced by synthetic ecteinascidins in melanoma and SCLC cells. **a, b** Heatmap showing average 18S-normalized expression ($n = 3$) of the indicated genes in 501mel **a** and MM029 **b** cells treated with either lurbinectedin, ecubectedin or PM54 (5xIC50 concentration) for the indicated period of time. Results were obtained by RT-qPCR and are shown as relative expression compared to DMSO-treated cells. RPL13a is a housekeeping gene. **c** Heatmap showing average 18S-normalized expression ($n = 3$) of the indicated genes in DMS53 cells (SCLC) treated with synthetic ecteinascidins (5xIC50 concentration (IC50 = 0.11 nM for lurbinectedin, 0.16 nM for ecubectedin and 0.15 nM for PM54)) for the indicated period of time. Results were obtained by RT-qPCR and are shown as relative expression compared to DMSO-treated cells. RPL13a is a housekeeping gene. **d** Upper panel: This analysis ($n = 3$) focuses on three gene sets: (1) genes commonly downregulated after treatment in melanoma, SCLC, and NSCLC cells, (2) putative super-enhancer-dependent genes in DMS53 SCLC

cells, and (3) genes whose expression exhibited a fold change between 0.9 and 1.1 relative to DMSO, which we considered unaffected by the treatment (GSE195663). These sets comprised the 648, 424, and 8435 genes, respectively. From these genes, we selected only the genes presenting H3K27ac peaks located at their transcription start sites (TSS), yielding 348 genes for the commonly downregulated genes across the three cancers, 424 for the SCLC super-enhancer-dependent genes, and 1434 for the unaffected genes (see Supplementary Data 7). Metaplot distribution shows H3K27ac signal in a ± 5 kb window around the TSS of these three groups of genes in mock- or lurbinectedin-treated DMS53 cells (GSE179074). Lower panel: Heatmap profiles representing the read density clusters obtained with seqMINER for the H3K27ac signal. **e** Gene tracks showing H3K27ac occupancy and RNA-Seq signals ($n = 3$) at the CDK8 (top), MYC (middle) and RPL13a (bottom) loci in mock- or lurbinectedin-treated DMS53 cells.

To analyze melanosphere viability after drug treatment, cells were treated with CellTiterGlo reagent (Promega) according to the manufacturer's instructions. Luminescence signals were measured with a Centro XS LB 960 microplate reader (Berthold).

Immunofluorescence assays

After PBS-rinsing, cells grown on coverslips were fixed with 4% paraformaldehyde for 15 min. Cells were then permeabilized with PBS and 0.1% Triton X-100. Blocking was done with 10% BSA. Primary antibodies were incubated overnight at 4 °C, after which cells were stained for 1 h at room temperature with AlexaFluor-conjugated secondary antibodies diluted in PBS + 10% FCS (Life technologies) and stained with DAPI. For BRD4 and MED1 foci quantifications, image acquisition was performed on a TCS SP5 inverted confocal microscope (Leica), and foci were counted using the Cell Counter plugin of the Fiji software.

For immunohistology, tumors were grown as mentioned above and were extracted after 24 h following a single dose of placebo treatment or 1.2 mg/kg of ecubectedin or PM54. In parallel, untreated tumors were extracted. The tumors were fixed in 10% formalin and embedded in paraffin for histology. Slides prepared from 5 μ m-thick paraffin sections were processed for antigen retrieval in 10 mM sodium citrate buffer (PH = 6.0) for 45 min at 95 °C in a water bath. The slides were cooled down at room temperature (RT) for 15 min. They were rinsed in PBS and then incubated in a humidified chamber for 16 h at 4 °C, with the primary antibodies diluted in PBS containing 0.1% (v/v) Tween 20 (PBST) to detect mitotic (pHH3-positive) and apoptotic (cleaved caspase 3-positive) cells. After rinsing in PBST, detection of the bound primary antibodies was performed for 1 h at room temperature in a humidified chamber using 555-conjugated secondary rabbit IgG antibody. The sections were then counterstained with DAPI to label nuclei. Stained sections were digitalized using a slide scanner (Nanozoomer 2.0-HT, Hamamatsu) and analyzed with the corresponding ND.View2 software.

Large 8-Bits digital scanned images of tumors stained for nuclei (10,000 to 30,000 nuclei per section) and pHH3 or cleaved caspase 3 were processed through an inhouse python (v3.8) algorithm to quantify positive cells. Basically, blue channels were proposed to a Cellpose2 model (deep learning model backbone by pytorch process) to segment nuclei. Subsequently, nuclei were analyzed for specific signals. For pHH3, a nucleus was considered positive if total pixels above 50 in intensity value exceeds 20% of nuclei surface (in 8 Bits image values range from 0 [no signal] to 255). Hence, we ensured that we did not consider unspecific background signals or insignificantly bright signals. The same procedure was applied to Caspase3 with pixel value set to 50 and minimal covered surface set to 30%. For each image, a ratio of positive cells/total nuclei was returned as the experimental variable. Statistics were produced using python's pingouin library (v0.5.3) with two-way ANOVA and post hoc tests being built-in functions.

High throughput sequencing

Supplementary Data 9 provides additional information about high throughput sequencing data, including among others, sequences quality controls, preprocessing, mapping, quantification and normalization methods, as well as size-number matched shuffled regions controls for Chem-Map data.

a. Bulk RNA-Seq and analysis. Library preparation was performed at the GenomEast platform at the Institute of Genetics and Molecular and Cellular Biology using TruSeq Stranded Total RNA Reference Guide - PN 1000000040499. Total RNA-Seq libraries were generated from 700 ng of total RNA using TruSeq Stranded Total RNA Library Prep Gold kit and TruSeq RNA Single Indexes kit A and B (Illumina, San Diego, USA), according to manufacturer's instructions. Briefly, cytoplasmic and mitochondrial ribosomal RNA (rRNA) was removed using biotinylated, target-specific oligos combined with Ribo-Zero rRNA removal beads. Following purification, the depleted RNA was fragmented into small pieces using divalent cations at 94 °C for 8 min. Cleaved RNA fragments were then copied into first strand cDNA using reverse transcriptase and random primers followed by second strand cDNA synthesis using DNA Polymerase I and RNase H. Strand specificity was achieved by replacing dTTP with dUTP during second strand synthesis. The double stranded cDNA fragments were blunted using T4 DNA polymerase, Klenow DNA polymerase and T4 PNK. A single 'A' nucleotide was added to the 3' ends of the blunt DNA fragments using a Klenow fragment (3' to 5'exo minus) enzyme. The cDNA fragments were ligated to double stranded adapters using T4 DNA Ligase. The ligated products were enriched by PCR amplification. Surplus PCR primers were further removed by purification using AMPure XP beads (Beckman-Coulter, Villepinte, France) and the final cDNA libraries were checked for quality and quantified using capillary electrophoresis. Libraries were sequenced on an Illumina HiSeq 4000 sequencer as single read 50 base reads. Image analysis and base calling were performed using RTA version 2.7.7 and bcl2fastq version 2.20.0.422.

Reads were preprocessed to remove adapter and low-quality sequences (Phred quality score below 20). After this preprocessing, reads shorter than 40 bases were discarded for further analysis. These preprocessing steps were performed using cutadapt version 1.10. Reads were mapped to rRNA sequences using bowtie version 2.2.8 and reads mapping to rRNA sequences were removed for further analysis. Reads were mapped onto the hg19 assembly of Homo sapiens genome using STAR version 2.5.3a. Gene expression quantification was performed from uniquely aligned reads using htseq-count version 0.6.1p1, with annotations from Ensembl version 75 and "union" mode. Only non-ambiguously assigned reads have been retained for further analyzes. Read counts have been normalized across samples with the median-of-ratios method proposed by Anders and Huber¹² to make these counts comparable between samples. Comparisons of interest were performed using the Wald test for differential expression⁴⁹ and implemented in the Bioconductor package DESeq2 version 1.16.1.

Genes with high Cook's distance were filtered out and independent filtering based on the mean of normalized counts was performed. *P*-values were adjusted for multiple testing using the Benjamini and Hochberg method⁵⁰. Deregulated genes were defined as genes with $\log_2(\text{Fold change}) > 1$ or < -1 and adjusted *P*-value < 0.05 .

Volcano plots were generated using the Prism9 statistical software (GraphPad). Heatmaps were generated using Morpheus (<https://software.broadinstitute.org/morpheus>). Venn diagrams were generated using DeepVenn (<http://www.deepvenn.com/>) and representation factors and hypergeometric *P*-values were determined using Graeber lab software (<https://systems.crump.ucla.edu/hypergeometric/>). GO Analysis was performed using ShinyGO. Metascape and enrichr analyzes can be found in Supplementary Data 9⁵¹. The number of assigned reads for each sample exceeds 15.10^6 (Supplementary Data 9), ensuring adequate coverage of the majority of expressed genes, with the exception of very low-expressed ones.

b. Chem-map and Cut&Tag. 501mel and MM029 cells were seeded and grown to sub-confluency in 15-cm plates before treatment for 8 h with DMSO, biotinylated lurbinedin (Bio-lurbi) or biotinylated PM54 (Bio-PM54) at a concentration equivalent to $10 \times \text{IC}_{50}$ (see Table 1). Chem-map (Biological triplicates) and CUT&TAG (Biological duplicates) were then performed using the Active Motif CUT&Tag-IT assay kit (53160, 53165), following the manufacturer's instructions. Briefly, 5×10^5 cells per condition were collected and washed twice before being bound to Concanavalin A beads and then incubated overnight at 4 °C with primary antibodies (1:50 dilutions). The following day, the corresponding guinea pig Anti-rabbit or rabbit Anti-mouse secondary antibodies were used at a 1:100 dilution in digitonin buffer and incubated at room temperature for 1 h. Subsequently, the CUT&Tag-IT Assembled pA-Tn5 Transposomes were incubated at room temperature for 1 h, and cells were resuspended in Tagmentation buffer and incubated at 37 °C for 1 h. The Tagmentation process was then stopped by adding EDTA and SDS. Protein digestion was performed by adding Proteinase K (10 mg/mL) and incubating at 55 °C for 1 h. The DNA was retrieved with DNA purification columns provided by the manufacturer and was then subjected to library preparation and PCR amplification and purified by 2 successive washes with SPRI beads. Libraries were sequenced on an Illumina NextSeq 2000 sequencer as paired-end 50 base reads. Image analysis and base calling were performed using RTA version 2.7.7 and BCL Convert version 3.8.4. The adapter sequence: CTGTCTCTTATA has been trimmed with cutadapt 1.18 with option: -a CTGTCTCTTATA -A CTGTCTCTTATA -m 5 -e 0.1 and Bowtie2⁵² parameter: -N 1 -X 1000, was used for mapping to the human genome (hg19). After the mapping, reads overlapping with ENCODE blacklist V2 were filtered. Each de-duplicated read was extended to its fragment size. Tracks were normalized with RPKM method. Peak calling was performed using Macs2 2.2.7.1⁵³ in BEDPE and narrow mode. narrowPeaks from biological triplicate samples were then merged to a single master peak set. BEDtools⁵⁴ was used to calculate the read coverage for each peak and for each sample. Peaks were annotated using Homer⁵⁵ software with ucsc 6.4 gene annotation. Promoters were defined as regions extending from 1 kb upstream to 100 bp downstream of the TSS and the "Annotate peaks" Homer tool was then employed to identify the promoters bound by the drugs. Bigwig tracks were generated using bamCoverage from deepTools 3.5.4⁵⁶ and normalized with RPKM method. The differential analysis was performed using DESeq2⁵⁷. Peak correlation analysis was performed using DiffBind⁵⁸ r package. Heatmap and average profile analyzes were performed using seqMINER⁵⁹ and deepTools. For Super-Enhancer calling, ROSE algorithm version 0.1 (http://younglab.wi.mit.edu/super_enhancer_code.html) was applied with default parameters (stitch distance = 12500^{8,60}) using the BRD4 or H3K27ac peaks identified by MACS2 with the Cut&Tag experiments. TSS regions (Refseq TSS ± 1000 bp) were excluded. We defined SEs as 'bona fide' if they

were positive for both H3K27ac and BRD4 signals. ROSE-gene mapper (Default parameters, hg19) was used to link super enhancers to targeted genes based on proximity and regulation potential. We considered Bio-lurbi or Bio-PM54 binding peaks to be overlapping with bona fide SEs if there was at least 1 bp of overlap. Similarly, all other overlapping analyzes considered different peaks as overlapping if there was at least 1 bp of overlap.

c. ATAC-Seq. 501mel and MM029 cells were seeded and grown to sub-confluency in 15-cm plates, and ATAC-Seq was then performed using the Active Motif ATAC-Seq Kit (53150), following the manufacturer's instructions. Briefly, 1×10^5 nuclei were isolated by adding 100 μL ice cold ATAC-lysis buffer to the cell pellet. After centrifugation (500 g, 10 min at 4 °C), cells were washed and incubated with the tagmentation master mix in a shaking heat block at 37 °C/200 g for 30 min. Obtained DNA was taken up in DNA purification buffer, purified using the contained DNA purification columns, amplified for 10 cycles using indexed primers, and size-selected using SPRI beads. Libraries were sequenced on an Illumina NextSeq 2000 sequencer as paired-end 50 base reads. Image analysis and base calling were performed using RTA version 2.7.7 and BCL Convert version 3.8.4. Samples were analyzed using the ENCODE ATACseq pipeline release v2.0.2 with hg19 assembly. All the experiments were performed in biological duplicates.

d. Shuffled analysis. To assess the specificity of signal enrichment, a control dataset was generated by using shuffled genomic regions for Bio-Ecteinascidins, ATAC-seq, CpG islands and super-enhancer peaks. The shuffling process was implemented using "bedtools shuffle" tool, which randomly redistributed the control regions across the genome while ensuring they did not overlap with the experimental regions. These shuffled regions were subjected to the same analysis pipeline as the targeted regions to serve as a negative control in downstream enrichment analysis.

Identification of active enhancers using ABC-scoring

The Active-By-Contact (ABC) model⁴³ was used to integrate ATAC-Seq, Cut&Tag and RNA-Seq data to generate a genome-wide annotation of all active cis-candidate regulatory regions (cCRE) directly implicated in activating gene expression in 501mel cells. First, candidate cCREs were identified using the makeCandidateRegions function which integrated ATAC-Seq narrow peaks and ATAC-Seq bam alignments. Settings were changed to 250 bp extension from the summit and peak strength equal to 1.5×10^5 . cCRE activity was then measured using the run.neighborhoods function where candidate cCREs were integrated with H3K27ac bam alignments, followed by an additional removal of cCREs linked to housekeeping genes whose activity may interfere with ones linked to cell-state/identity genes. Next, we estimated the ABC power law score using the predict function. Here, the obtained cCREs were assessed for their predicted physical contacts with nearby genes based on HiC data. HiC parameters were obtained using the juicebox_dump and compute_powerlaw_fit_from_hic functions and a publicly available SKMEL-5 (differentiated melanoma cells) HiC h5 matrix (GSE105491⁴⁴), used to train the model. This HiC matrix was converted into juicer format using hic-converter (<https://github.com/4DGB/hic-converter>). HiC parameters were set as follows: --hic_gamma 0.9456060921860431, --hic_scale 5.081208553261949, --hic_gamma_reference 0.87, --hic_pseudocount_distance 5000. All putative cCREs were filtered using the filter_prediction script, and setting an ABC-score threshold of 0.02 we removed self-promoter contacts and retained only cCREs linked to expressed genes. Using R, cCREs were ranked based on their final ABC-scores measured as the sum of the ABC-score values of their related genes. Differentially expressed genes determined by RNA-Seq were used to identify their associated promoter-cCRE interactions. Plots were generated using R and GraphPad Prism.

RNA extraction and RT-qPCR

Total RNA isolation was performed according to the manufacture protocol with NucleoSpin RNA Plus kit (Macherey-Nagel). RNA was retrotranscribed with Reverse Transcriptase Superscript IV (Invitrogen), qPCR was performed with SYBR Green (Roche) and on a Light-Cycler 480 (Roche). Target gene expression was normalized using 18S as reference gene.

ChIP-qPCR

501mel and MM029 cells were seeded and grown to sub-confluency in 15-cm plates. After drug treatments, cells were fixed with 0.4 % PFA for 10 min and quenched with 2 M Glycin pH 8. Cells pellets were lysed in 25 mM HEPES pH 7.8, 10 mM NaCl, 1.5 mM MgCl₂, 0.5 % NP-40, 1 mM DTT. Nuclei were resuspended in 50 mM Hepes-KOH pH 7.8, 140 mM NaCl, 1 mM EDTA, 1% Triton X-100, 0.1 mM Na-deoxycholate, 0.1 % SDS and sonicated at 4 °C with a Q500 sonicator (Qsonica) to get DNA fragments between 100-500 bp. 50 µg of the sonicated chromatin was then diluted in Dilution buffer (1 % Triton X-100, 2 mM EDTA, 20 mM Tris HCl pH 7.5, 150 mM NaCl) and incubated overnight at 4 °C with 5 µg of respective antibodies. The antibody-chromatin complex was then captured with a mix of protein A and G Dynabeads (Invitrogen) for 2 h at 4 °C, and beads were then washed twice in Low Salt Washing Buffer (1 % Triton, 2 mM EDTA, 20 mM Tris HCl pH 7.5, 150 mM NaCl, 0.1 % SDS), High salt Washing Buffer (1 % Triton, 2 mM EDTA, 20 mM Tris HCl pH 7.5, 500 mM NaCl, 0.1 % SDS), and TE buffer (100 mM Tris HCl pH 7.5, 10 mM EDTA). Immunoprecipitated chromatin was subsequently eluted from beads in 1 % SDS and 100 mM NaHCO₃ at 65 °C for 30 min, and crosslinks were reversed by overnight incubation with Proteinase K (50 µg/ml) at 65 °C. The DNA was finally purified with the QIAquick PCR Purification kit (QIAGEN), resuspended in 200 µL of water, and analyzed by qPCR. Quantification of ChIP DNA concentrations with qPCR was performed by calculating the percent of input for each ChIP sample, calculated as $2^{-(Ct_{input} - Ct_{IP})} \times 100$. Subsequently, the obtained percentage was normalized to the negative control IgG. Finally, the fold enrichment of the drug-treated samples over the DMSO-treated samples was calculated.

Animal studies. Animal studies were carried out at PharmaMar, which complies with ethical standards and principles governing the use of animal models. 4- to 6-week-old NSG (Charles River laboratory) or athymic nude female (Inotiv laboratory) mice were subcutaneously implanted into their right flank with human melanoma cell suspensions (LOX-IMVI, WM-266-4, 501mel, or 501mel^{Vemur}). Athymic nude mice were used for their lack of T-cell mediated immunity, which is suitable for studies requiring longer-term tumor growth observations (LOX-IMVI and WM-266-4). NSG mice were chosen for their more severely compromised immune systems, which allow for robust engraftment and growth of human melanoma cells, including those resistant to therapies (501mel and 501mel^{Vemur}). The experiments performed in this study is not affected by sex of the animal, consequently only females were used. When tumors began to develop, these were measured 2-3 times per week. Tumor volume was calculated with the equation $(a \times b^2)/2$, where “a” and “b” referred to the longest and shortest diameters, respectively. When tumors reached a size of 150 mm³, tumor bearing animals ($N=8$ /group) were treated with placebo (saline solution) or ecubectedin or PM54 at 1.2 mg/kg weekly. Tumor volume and animal body weights were measured 2–3 times per week, starting from the first day of treatment. The median was determined for tumor volume/size on each measurement day. Treatment tolerability was assessed by monitoring body weight evolution, clinical signs of systemic toxicity, as well as evidences of local damage in the injection site. Differences on antitumor effect were evaluated by comparing tumor volume data as well as median survival time from the placebo-treated group with Ecubectedin or PM54 treated groups. For this, a two-tailed Mann-Whitney U test was used. According to animal care and enforcement, the maximum allowable diameter for

subcutaneous tumors in mice is 20 mm. This limit was not exceeded at any point. All animals used in this research were housed in a specific pathogen-free (SPF) environment with a 12 h dark/light cycle, constant and appropriate room temperature (22–25 °C), with relative humidity between 55 ± 10% and had free access to food and water.

Antibodies dilutions. ACTb, WB Dilution 1/1000, Cat# 558623, RRID:AB_1645341; ATM, WB Dilution 1/1000, Cat# 2873S, RRID:AB_2062659; AXL, WB Dilution 1/1000, Cat# 13196-1-AP RRID:AB_10642006; Biotin, 2.5µg/ ChIP-CUT&Tag assay, Cat# 5597S, RRID:AB_10828011; BRD4, 2.5µg/ ChIP-CUT&Tag assay, Cat# 39909, RRID:AB_2615059; CDK12, WB Dilution 1/1000, Cat# ABE1861; CDK13, WB Dilution 1/1000, Cat# ABE1860; CDK7, WB Dilution 1/2000, Cat# 556345, RRID:AB_396374; Cleaved Caspase-3 (Asp175), WB Dilution 1/2000, Cat# 9661S RRID:AB_2341188; EGFR, WB Dilution 1/2000 Cat# sc-373746, RRID:AB_10920395; EP300, WB Dilution 1/1000 Cat# 61401, RRID:AB_2716754; H3K27ac, 1µg/ChIP-CUT&Tag assay, Cat# 91193, RRID:AB_2793797; H3K27me3, 1 µg/ChIP-CUT&Tag assay, 9733, RRID:AB_2616029; IRF1, WB Dilution 1/2000, Cat# 8478S RRID:AB_10949108; MED1, WB Dilution 1/1000, Cat# ab64965, AB_1142301; MITF, WB Dilution 1/2000, Cat# 12590S, RRID:AB_2616024; MYC, WB Dilution 1/1000, Cat# sc-764, RRID:AB_631276; PD-L1, WB Dilution 1/2000 Cat# 13684S, RRID:AB_2687655; Phospho-ATM (Ser1981), WB Dilution 1/2000, Cat# 13050S, RRID:AB_2798100; Phospho-Histone H3 (Ser10), WB Dilution 1/2000, Cat# 06-570, RRID:AB_310177; Phospho-Stat1 (Tyr701), WB Dilution 1/1000, Cat# 9167S, RRID:AB_561284; yH2AX, WB and IF Dilution 1/1000, Cat# AB22551, RRID:AB_447150; RPB1, 2.5µg/ ChIP-CUT&Tag assay, Cat# AF6851, RRID:AB_2847574; RPB1, 2.5µg/ ChIP-CUT&Tag assay, Cat# AF6851, RRID:AB_2847574; SOX10, WB Dilution 1/1000, Cat# sc-365692, RRID:AB_10844002; SOX9, WB Dilution 1/1000 Cat# 82630S, RRID:AB_2665492; STAT1, WB Dilution 1/1000, Cat# 14994S, RRID:AB_2737027; Vinculin, WB Dilution 1/1000, Cat# V4505-100UL, RRID:AB_477617

Statistics and reproducibility

Experimental data was plotted and analyzed using either Excel (Microsoft) or GraphPad Prism (GraphPad Software Inc.). The tests used included ordinary one-way ANOVA using Dunnett’s multiple comparisons test, Logrank (Mantel-Cox) test, Hypergeometric distribution test, One-way ANOVA with post-hoc Tukey adjustment comparisons, the Benjamini and Hochberg test method, the Fisher’s Exact Test, and the Wald test. Differences were considered significant at $P < 0.05$. Each in vitro experiment was repeated independently at least three times unless indicated differently. The number of samples and replicates are indicated in the respective figure legends. No data were excluded from the analyzes. These experiments do not require blinding of the investigator.

Resource availability

Lead contact. Further information and requests for resources and reagents should be directed to and will be fulfilled by the Lead Contact, Frédéric Coin (fredr@igbmc.fr). All data are available in the Source Data File.

Extended resource table. An extended resource table with antibodies, oligonucleotide sequences, chemicals and reagents used in this work is provided in Supplementary Data 8.

Reporting summary

Further information on research design is available in the Nature Portfolio Reporting Summary linked to this article.

Data availability

The publicly available data used in this study are available in the GEO database under the following accession codes: the RNA-seq, ChIP-seq and ATAC-seq data from SCLC cell lines; [GSE179074](https://www.ncbi.nlm.nih.gov/geo/query/acc.cgi?acc=GSE179074)³⁵ and

GSE195663³⁵, the RNA-seq data from the MM047 cell line; GSE205463⁴², the ATAC-seq and CUT&Tag data from the ECC4, A99 and DMS53 cell lines; GSE190618⁴¹, and the SKMEL-5 (differentiated melanoma cells) HiC h5 matrix GSE105491⁴⁴. The raw RNA-seq, ATAC-seq, and Cut&Tag data generated in this study have been deposited at GEO under accession numbers GSE256100 and GSE256094. The remaining data are available within the Article, Supplementary Information or Source Data file. Source data are provided with this paper.

References

- Bradner, J. E., Hnisz, D. & Young, R. A. Transcriptional Addiction in Cancer. *Cell* **168**, 629–643 (2017).
- Sengupta, S. & George, R. E. Super-Enhancer-Driven Transcriptional Dependencies in Cancer. *Trends Cancer* **3**, 269–281 (2017).
- Zanconato, F. et al. Transcriptional addiction in cancer cells is mediated by YAP/TAZ through BRD4. *Nat. Med* **24**, 1599–1610 (2018).
- Hogg, S. J., Beavis, P. A., Dawson, M. A. & Johnstone, R. W. Targeting the epigenetic regulation of antitumour immunity. *Nat. Rev. Drug Discov.* **19**, 776–800 (2020).
- Vervoort, S. J. et al. Targeting transcription cycles in cancer. *Nat. Rev. Cancer* **22**, 5–24 (2022).
- Pott, S. & Lieb, J. D. What are super-enhancers? *Nat. Genet* **47**, 8–12 (2015).
- Hnisz, D. et al. Super-enhancers in the control of cell identity and disease. *Cell* **155**, 934–947 (2013).
- Whyte, W. A. et al. Master transcription factors and mediator establish super-enhancers at key cell identity genes. *Cell* **153**, 307–319 (2013).
- Sabari, B. R. et al. Coactivator condensation at super-enhancers links phase separation and gene control. *Science* **361**, eaar3958 (2018).
- Boija, A., Klein, I. A. & Young, R. A. Biomolecular Condensates and Cancer. *Cancer Cell* **39**, 174–192 (2021).
- Laham-Karam, N., Pinto, G. P., Poso, A. & Kokkonen, P. Transcription and Translation Inhibitors in Cancer Treatment. *Front. Chem.* **8**, 276 (2020).
- Bushweller, J. H. Targeting transcription factors in cancer — from undruggable to reality. *Nat. Rev. Cancer* **19**, 611–624 (2019).
- Kwiatkowski, N. et al. Targeting transcription regulation in cancer with a covalent CDK7 inhibitor. *Nature* **511**, 616–620 (2014).
- Berico, P. et al. CDK7 and MITF repress a transcription program involved in survival and drug tolerance in melanoma. *EMBO Rep.* <https://doi.org/10.15252/embr.202051683> (2021).
- Fontanals-Cirera, B. et al. Harnessing BET Inhibitor Sensitivity Reveals AMIGO2 as a Melanoma Survival Gene. *Mol. Cell* **68**, 731–744.e9 (2017).
- Donati, B., Lorenzini, E. & Ciarrocchi, A. BRD4 and Cancer: going beyond transcriptional regulation. *Mol. Cancer* **17**, 164 (2018).
- Hoek, K. S. et al. In vivo switching of human melanoma cells between proliferative and invasive states. *Cancer Res.* **68**, 650–656 (2008).
- Verfaillie, A. et al. Decoding the regulatory landscape of melanoma reveals TEADS as regulators of the invasive cell state. *Nat. Commun.* **6**, 6683 (2015).
- Wouters, J. et al. Robust gene expression programs underlie recurrent cell states and phenotype switching in melanoma. *Nat. Cell Biol.* **22**, 986–998 (2020).
- Pozniak, J. et al. A TCF4-dependent gene regulatory network confers resistance to immunotherapy in melanoma. *Cell* **187**, 166–183.e25 (2024).
- Gide, T. N., Wilmott, J. S., Scolyer, R. A. & Long, G. V. Primary and Acquired Resistance to Immune Checkpoint Inhibitors in Metastatic Melanoma. *Clin. Cancer Res.* **24**, 1260–1270 (2018).
- Weiss, S. A., Wolchok, J. D. & Sznol, M. Immunotherapy of Melanoma: Facts and Hopes. *Clin. Cancer Res.* **25**, 5191–5201 (2019).
- Schadendorf, D. et al. Melanoma. *Lancet* **392**, 971–984 (2018).
- Jerby-Amon, L. et al. A Cancer Cell Program Promotes T Cell Exclusion and Resistance to Checkpoint Blockade. *Cell* **175**, 984+ (2018).
- Tsoi, J. et al. Multi-stage Differentiation Defines Melanoma Subtypes with Differential Vulnerability to Drug-Induced Iron-Dependent Oxidative Stress. *Cancer Cell* **33**, 890–904.e5 (2018).
- Arozarena, I. & Wellbrock, C. Phenotype plasticity as enabler of melanoma progression and therapy resistance. *Nat. Rev. Cancer* **19**, 377–391 (2019).
- Benboubker, V., Boivin, F., Dalle, S. & Caramel, J. Cancer Cell Phenotype Plasticity as a Driver of Immune Escape in Melanoma. *Front. Immunol.* **13**, 873116 (2022).
- Chauhan, J. S., Hölzel, M., Lambert, J., Buffa, F. M. & Goding, C. R. The MITF regulatory network in melanoma. *Pigment Cell Melanoma Res* **35**, 517–533 (2022).
- Comandante-Lou, N., Baumann, D. G. & Fallahi-Sichani, M. AP-1 transcription factor network explains diverse patterns of cellular plasticity in melanoma cells. *Cell Rep.* **40**, 111147 (2022).
- Karras, P. et al. A cellular hierarchy in melanoma uncouples growth and metastasis. *Nature* **610**, 190–198 (2022).
- Hoek, K. S. & Goding, C. R. Cancer stem cells versus phenotype-switching in melanoma. *Pigment Cell Melanoma Res* **23**, 746–759 (2010).
- Rambow, F., Marine, J. C. & Goding, C. R. Melanoma plasticity and phenotypic diversity: therapeutic barriers and opportunities. *Genes Dev.* **33**, 1295–1318 (2019).
- Molinski, T. F., Dalisay, D. S., Lievens, S. L. & Saludes, J. P. Drug development from marine natural products. *Nat. Rev. Drug Discov.* **8**, 69–85 (2009).
- Santamaria Nunez, G. et al. Lurbinectedin Specifically Triggers the Degradation of Phosphorylated RNA Polymerase II and the Formation of DNA Breaks in Cancer Cells. *Mol. Cancer Ther.* **15**, 2399–2412 (2016).
- Costanzo, F. et al. Promoters of ASCL1- and NEUROD1-dependent genes are specific targets of lurbinectedin in SCLC cells. *EMBO Mol. Med* <https://doi.org/10.15252/emmm.202114841> (2022).
- Trigo, J. et al. Lurbinectedin as second-line treatment for patients with small-cell lung cancer: a single-arm, open-label, phase 2 basket trial. *Lancet Oncol.* **21**, 645–654 (2020).
- Widmer, D. S. et al. Systematic classification of melanoma cells by phenotype-specific gene expression mapping. *Pigment Cell Melanoma Res* **25**, 343–353 (2012).
- David-Cordonnier, M.-H. et al. DNA and Non-DNA Targets in the Mechanism of Action of the Antitumor Drug Trabectedin. *Chem. Biol.* **12**, 1201–1210 (2005).
- Couto, G. K. et al. The Melding of Drug Screening Platforms for Melanoma. *Front. Oncol.* **9**, 512 (2019).
- Casper, D. J. et al. Use of Anti-phosphohistone H3 Immunohistochemistry to Determine Mitotic Rate in Thin Melanoma. *Am. J. Dermatopathol.* **32**, 650–654 (2010).
- Yu, Z. et al. Chem-map profiles drug binding to chromatin in cells. *Nat. Biotechnol.* **41**, 1265–1271 (2023).
- Berico, P. et al. Super-enhancer-driven expression of BAHCC1 promotes melanoma cell proliferation and genome stability. *Cell Rep.* **42**, 113363 (2023).
- Fulco, C. P. et al. Activity-by-contact model of enhancer–promoter regulation from thousands of CRISPR perturbations. *Nat. Genet* **51**, 1664–1669 (2019).
- The ENCODE Project Consortium. An integrated encyclopedia of DNA elements in the human genome. *Nature* **489**, 57–74 (2012).
- Zawistowski, J. S. et al. Enhancer Remodeling during Adaptive Bypass to MEK Inhibition Is Attenuated by Pharmacologic Targeting of the P-TEFb Complex. *Cancer Discov.* **7**, 302–321 (2017).
- Le, V. H., Inai, M., Williams, R. M. & Kan, T. Ecteinascidins. A review of the chemistry, biology and clinical utility of potent tetrahydroisoquinoline antitumor antibiotics. *Nat. Prod. Rep.* **32**, 328–347 (2015).

47. Xie, W. et al. Lurbinectedin synergizes with immune checkpoint blockade to generate anticancer immunity. *Oncimmunology* **8**, e1656502 (2019).
48. Dumoulin, D. W. et al. Lurbinectedin shows clinical activity and immune-modulatory functions in patients with pre-treated small cell lung cancer and malignant pleural mesothelioma. *Eur. J. Cancer* **172**, 357–366 (2022).
49. Love, M. I., Huber, W. & Anders, S. Moderated estimation of fold change and dispersion for RNA-seq data with DESeq2. *Genome Biol.* **15**, 1–21 (2014).
50. Benjamini, Y. & Hochberg, Y. Controlling the False Discovery Rate: A Practical and Powerful Approach to Multiple Testing. *J. R. Stat. Soc.: Ser. B (Methodol.)* **57**, 289–300 (1995).
51. Ge, S. X., Jung, D. & Yao, R. ShinyGO: a graphical gene-set enrichment tool for animals and plants. *Bioinformatics* **36**, 2628–2629 (2020).
52. Langmead, B. & Salzberg, S. L. Fast gapped-read alignment with Bowtie 2. *Nat. Methods* **9**, 357–359 (2012).
53. Zhang, Y. et al. Model-based analysis of ChIP-Seq (MACS). *Genome Biol.* **9**, R137 (2008).
54. Quinlan, A. R. & Hall, I. M. BEDTools: a flexible suite of utilities for comparing genomic features. *Bioinformatics* **26**, 841–842 (2010).
55. Heinz, S. et al. Simple Combinations of Lineage-Determining Transcription Factors Prime cis-Regulatory Elements Required for Macrophage and B Cell Identities. *Mol. Cell* **38**, 576–589 (2010).
56. Ramírez, F. et al. deepTools2: a next generation web server for deep sequencing data analysis. *Nucleic Acids Res* **44**, W160–W165 (2016).
57. Love, M. I., Huber, W. & Anders, S. Moderated estimation of fold change and dispersion for RNA-seq data with DESeq2. *Genome Biol.* **15**, 550 (2014).
58. Ross-Innes, C. S. et al. Differential oestrogen receptor binding is associated with clinical outcome in breast cancer. *Nature* **481**, 389–393 (2012).
59. Ye, T. et al. seqMINER: an integrated ChIP-seq data interpretation platform. *Nucleic Acids Res.* **39**, e35–e35 (2011).
60. Loven, J. et al. Selective inhibition of tumor oncogenes by disruption of super-enhancers. *Cell* **153**, 320–334 (2013).
61. Horie, M. et al. An integrative epigenomic approach identifies *ELF3* as an oncogenic regulator in *ASCL1*-positive neuroendocrine carcinoma. *Cancer Sci.* **114**, 2596–2608 (2023).

Acknowledgements

This study was supported by the Ligue contre le cancer (Equipe Labélisée 2022-2024), the Institut National du Cancer (INCa) (INCa_18353), the grant ANR-10-LABX-0030-INRT, a French State fund managed by the Agence Nationale de la Recherche under the frame program Investissements d’Avenir ANR-10-IDEX-0002-02. This work of the Interdisciplinary Thematic Institute IMCBio+, as part of the ITI 2021-2028 program of the University of Strasbourg, CNRS and Inserm, was supported by IdEx Unistra (ANR-10-IDEX-0002), and by SFRI-STRAT’US project (ANR-20-SFRI-0012) and EUR IMCBio (ANR-17-EURE-0023) under the framework of the France 2030 Program. Sequencing was performed by the IGBMC GenomEast platform, a member of the “France Génomique” consortium (ANR-10-INBS-0009). Histology and subsequent image analysis were performed by the pathology facility of the mouse clinic institute (ICS), a member of the Celphedia/Phenomin infrastructures

(ANR-10-INBS-0007). We also thank the IGBMC PluriCell East facility, Flow cytometry and Photonic microscopy services. P.B is supported by the Ligue contre le Cancer. JME was sponsored by a Mount Jade Scholar Fellow from the MOST of Taiwan and a Yonglin Chair Professor grant of National Taiwan University. We thank Dr Hsiang-Hung Huang for having initiated the work on SCLC cells.

Author contributions

Conceptualization: FC. Methodology: MC, JO, ID, C-Cuevas, FC. Investigation: MC, JO, MN, LS, PC, PB, C-Capelli, CM, AZ, CE, MJGN, TKL, EC, PA, MMD and GSN. Analysis of data: TY, GD, JME. Funding acquisition: FC. Supervision: FC. Writing – original draft: FC. Writing – review & editing: ID, EC, CC, MC, JO.

Competing interests

PA and C-Cuevas are PharmaMar S.A employees and shareholders. MJGN, MMD, GSM are PharmaMar employees. The remaining authors declare no competing interests.

Additional information

Supplementary information The online version contains supplementary material available at <https://doi.org/10.1038/s41467-024-55667-z>.

Correspondence and requests for materials should be addressed to Frédéric Coin.

Peer review information *Nature Communications* thanks the anonymous reviewers for their contribution to the peer review of this work. A peer review file is available.

Reprints and permissions information is available at <http://www.nature.com/reprints>

Publisher’s note Springer Nature remains neutral with regard to jurisdictional claims in published maps and institutional affiliations.

Open Access This article is licensed under a Creative Commons Attribution-NonCommercial-NoDerivatives 4.0 International License, which permits any non-commercial use, sharing, distribution and reproduction in any medium or format, as long as you give appropriate credit to the original author(s) and the source, provide a link to the Creative Commons licence, and indicate if you modified the licensed material. You do not have permission under this licence to share adapted material derived from this article or parts of it. The images or other third party material in this article are included in the article’s Creative Commons licence, unless indicated otherwise in a credit line to the material. If material is not included in the article’s Creative Commons licence and your intended use is not permitted by statutory regulation or exceeds the permitted use, you will need to obtain permission directly from the copyright holder. To view a copy of this licence, visit <http://creativecommons.org/licenses/by-nc-nd/4.0/>.

© The Author(s) 2025

¹IGBMC, Institut de Génétique et de Biologie Moléculaire et Cellulaire Illkirch Cedex, C.U. Equipe Labélisée Ligue contre le Cancer, Strasbourg, France.

²UMR7104, Illkirch, France. ³U1258, Illkirch, France. ⁴Université de Strasbourg, Illkirch, France. ⁵Department of Pathology, New York University Grossman School of Medicine, New York, USA. ⁶Interdisciplinary Melanoma Cooperative Group, Perlmutter Cancer Center, NYU Langone Health, New York, USA. ⁷Cell Biology Department, Research and Development, PharmaMar SA, Colmenar Vejo, Spain. ⁸Graduate Institute of Microbiology, College of Medicine, National Taiwan University, Taipei, Taiwan. ⁹College of Medicine, National Taiwan University, Taipei city, Taiwan. ¹⁰These authors contributed equally: Max Cigrang, Julian Obid. ✉ e-mail: fredr@igbmc.fr